Available online at www.CivileJournal.org

Civil Engineering Journal

(E-ISSN: 2476-3055; ISSN: 2676-6957)

Vol. 10, No. 08, August, 2024

Shear Performance of Deep Concrete Beams with Openings Using Waste Tyre Steel Fibres: FEM and ANN Analysis

Daudi Salezi Augustino [1*]

[1] *Department of Structural and Construction Engineering, University of Dar es Salaam, 35131, Dar es Salaam, Tanzania.*

Received 30 April 2024; Revised 22 June 2024; Accepted 22 July 2024; Published 01 August 2024

Abstract

The creation of transverse openings in beams triggers the shear performance. The dual impact of height and length on the overall shear performance and strain variations in reinforcements of deep concrete beams with and without fibres was assessed to investigate the effect of opening in the beam. This effect of opening was explored and modelled using finite element software Abaqus and predicted using an artificial neural network (ANN) model. The data set for ANN was 56 deep concrete beams, while for the finite element model (FEM), 12 deep concrete beams were used. The effect of input parameters in the ANN model was assessed through sensitivity analysis. Results show that with an increase in opening depth, the strain in top steel reinforcement shifted to tensile strain, resulting in premature beam failure. In addition, experimental and FEM shear resistance had a mean absolute error (MAE) of 4.1, 5.0, and 20.6% for deep beams without fibres, with fibres and fibre mesh, respectively. Compared to available analytical models, the ANN model reasonably predicts the shear resistance with an R^2 of 0.84 and a mean square error (MSE) of 0.01. The use of the ANN and FEM models is recommended as they save time, and the prediction does not involve degradation of the environment, hence demonstrating sustainable construction practices.

Keywords: Sensitivity Analysis; Shear Resistance; Artificial Neural Network (ANN); Reinforced Concrete Deep; Finite Element Model.

1. Introduction

Transverse openings in reinforced concrete structural elements, such as beams with high depth, are provided for service utilities. The reasons for creating these openings are primarily architectural reasons, i.e., not to decrease the headroom if services utilities such as fire pipes are to be placed beneath the beam. These openings, particularly in the shear zone of the concrete beams, may lead to nonlinear responses and stress concentration at the openings' corners [1]. In practice, several researchers have developed analytical models to design deep concrete beams with transverse openings. The predictive model by Kong et al. (1975) [2] is among the prominent predictive models for estimating the shear resistance of deep concrete beams with transverse openings and without fibres. Due to only consideration of the height effect in model formulation, the Kong et al. (1975) model underrates the shear resistance. The model by Dang et al. (2021) [3] considered the outcome of stress along the concrete-fibre interface. However, the opening effect was yet to be expressed since the creation of the transverse opening, the shear transmission to support changes. The model [4] considered the opening effect; nevertheless, no impact of fibres was considered, and the model did not involve other parameters affecting shear performance. Instead, experimental shear resistance was used in model development and validation. For opening to affect shear transfer, a beam's line of force should be interrupted. The model by Smarzewski (2018) [5] had an opening and fibres in the deep concrete beam; however, to some extent, it overestimates the shear performance once the opening is positioned in unloaded quadrants without intercepting the strut line of force. The

* Corresponding author: augustino.daudi@udsm.ac.tz

http://dx.doi.org/10.28991/CEJ-2024-010-08-02

© 2024 by the authors. Licensee C.E.J, Tehran, Iran. This article is an open access article distributed under the terms and conditions of the Creative Commons Attribution (CC-BY) license (http://creativecommons.org/licenses/by/4.0/).

models by Dang et al. (2021) [3] and Hussein & Abbas (2022) [4] were further developed in Augustino et al. [6] to capture the fibre-concrete interface, the orientation factor of traverse opening, the effect of steel reinforcement, and the grade of concrete.

Despite that, the analytical model by Augustino et al. [6] predicts well the shear resistance, the underlying assumption in the model formulation might not accurately capture the nonlinear behaviour and stress concentration as the upper part of the transverse opening rotates [1]. For instance, the FE model [7] predicts much better than the analytical models [2, 8]. This shows that non-linear behaviour can quickly be revealed and comprehended through the use of finite element modelling (FEM). The study by Saleh et al. [9] reveals that the FE model can effectively investigate the behaviour of reinforced deep concrete beams with transverse openings, overcoming their complexity, such as stress around the opening corners. Finite element modelling (FEM) is a crucial aspect of understanding the general response of structural elements, such as beams, that cannot be comprehended through experimental tests. The model considers the contribution of responses of individual discrete elements making up a beam. The selection elements that discretise the continuum solid beam depend on whether the model is in 2D or 3D domains. Through these elements, the analysis step is assigned, in which the Gauss integration points are used to estimate the finite element solution [10, 11]. Since the finite element method is an approximation method of analysis using shape functions, the proper selection of the finite element and Gauss points is essential for the convergence of the solution and to avoid spurious zero-energy modes [12, 13]. Since FEM is an approximation method that demands careful formulation or more space in computer drives, the necessity of using current technologically advanced models, such as neural networking models, to improve prediction has gained a pace [14]. Machine learning can replace empirical and semi-empirical prediction models currently used in practice. However, careful selection of ANN is vital to improve the predictive efficiency [15–17]. Among many available algorithms, the Levenberg-Marquardt algorithm is often used to find the minimum function (linear and nonlinear) over the space of parameters that increase stability and fast convergence [18–20]. The ensemble machine learning model can predict the shear resistance of the deep concrete beam with the opening [21]. Nevertheless, the orientation factor of the traverse opening was not taken into account, which detrimentally affected the overall shear performance of the structural elements, such as beams and columns [7, 22].

Current studies [23–28] have explored the significance of fibres on the mechanical properties of concrete at the material level. At the element level, despite the intensive studies on deep concrete beams with and without fibres, the studies quantified the contribution of the opening size and its location, compressive strength, and effect on reinforcement ratios. None have investigated the impact of waste steel fibres and dual-effect transverse opening height and length on strain variations along main and compressive steel reinforcement using finite element modelling. The strains in main and compressive steel reinforcement can indicate the active dowel action and compressive stress at the nominal axial strength of the boundary strut of the beam, respectively, that contribute to the shear-carrying capacity of the beam [29]. To gain insight into the nominal strength of the strut of a deep concrete beam, finite element modelling is a paramount tool for assessment, mainly when the beam involves opening. In addition, available artificial neural network models have yet to capture the orientation factor of transverse opening dimensions on the prediction of shear resistance of deep concrete beams with transverse openings [21, 30, 31]. Factors affecting the shear performance of deep concrete beams go beyond the known parameters, such as stirrup ratio, compressive strength of concrete, and dowel action of main steel reinforcement. Therefore, the sensitivity of factors such as the dual effect of opening length and height and the ratio of opening area to that of shear area must be established to precisely predict the shear performance of deep concrete beams.

1.1. Research Significance

The study utilises several sets of square and rectangular transverse openings of the exact sizes in the shear zone of a deep concrete beam. The study will use the Finite Element Model to explore the dual effect of opening length and height on the overall shear performance and strain variations in reinforcements of deep concrete beams with and without fibres. The study will provide the sensitivity of the dual effect of opening length and height (orientation factor of traverse opening) and the ratio of opening area to shear area on predicting the shear resistance of a deep concrete beam using the ANN model. The study will be beneficial to structural engineers regarding the possible reduction in shear resistance as the orientation factor increases and on critical areas that demand more attention to structural steel detailing.

2. Research Methodology

2.1. Finite Element Modelling

2.1.1. Material Parameters

In modelling, the Abaqus software was used, and the experimental shear capacity was based on a past study by Augustino et al. [1] and ABAQUS [32]. The concrete had a mean cylindrical compressive strength of 51.59 and 60.06 MPa for control beams and beams with fibres, respectively. The fibres used in concrete were 1.3 mm in diameter, 50 mm in length, and 0.5% fibre quantity. The model was established using the ultimate experimental results of the concrete cylinder. From the ultimate compressive stress of the curve, the descending part of the curve was based on the models by Saabye and Petersson [11] and Schneidera et al. [12] as in Equations 1 and 2. This study assumes that the compressive elastic modulus equals the tensile elastic modulus for compatibility reasons. The assumption has also been used by Kanos et al. [33]. Equation 3 and the constitutive model by Rai [34] (Equation 4) were used to establish the tensile behaviour of concrete and the tension-softening part of the stress-strain curve, respectively. The peak tensile strains used in the study were 0.000144 and 0.00015 for the beam with and without fibres, respectively.

$$\sigma = \left(\frac{m\beta(\varepsilon/\varepsilon_{peak})}{m\beta-1+(\varepsilon/\varepsilon_{peak})^{m\beta}}\right) \times \sigma_{peak} \tag{1}$$

$$\beta = \frac{1}{1-\frac{\sigma_{peak}}{E_0\varepsilon_{peak}}} \tag{2}$$

$$\sigma_t = \varepsilon E_0 \quad \text{for } \varepsilon \leq \varepsilon_{t,peak} \tag{3}$$

$$\sigma_t = \sigma_{to}\left(\frac{\varepsilon_{t,peak}}{\varepsilon}\right)^{0.4} \text{ for } \varepsilon \geq \varepsilon_{t,peak} \tag{4}$$

where, σ is the compressive stress of concrete, m is the material parameter that depends on the strength of the material (it is equal to one for concrete cylinder strength less than 62 MPa, β is the material parameter that depends on the shape of the stress-strain curve, ε is the total strain of concrete at a particular point, E_0 is the initial tangential modulus of concrete, σ_{peak} is the ultimate compressive stress of concrete and ε_{peak} is strain correspond to σ_{peak}, ε is the total tensile strain, σ_{to} is the tensile strength of concrete and σ_t is tensile stress at any point. To establish the post-behaviour of concrete, the stress-inelastic (crushing and cracking) strain curves were developed using Equations 5 and 6, respectively.

$$\varepsilon^{in} = \varepsilon - \frac{\sigma_c}{E_0} \tag{5}$$

$$\varepsilon^{cr} = \varepsilon - \frac{\sigma_t}{E_0} \tag{6}$$

where ε^{in} is the inelastic crushing strain, ε is the total strain in compression or tension loading setup, σ_c is the compressive stress in the yield point, E_0 is the initial modulus of elasticity for the undamaged material corresponding to a linear elastic zone and σ_t is the tensile strength of concrete. Since the crushing and cracking strain is defined, damage aspects of concrete that correlate with concrete's inelastic behaviour have to be modelled and defined using Equation 7.

$$d_{t,c} = 1 - \frac{\sigma}{\sigma_{peak}} \tag{7}$$

In these Equations, σ_{peak} is a peak tensile or compressive stress of the concrete test specimen, $d_{c,t}$ is a damage variable in compression or tension in the descending part of the stress-strain curve. It ranges from zero for undamaged to one for completely damaged material. The plastic strains are established in Equations 8 and 9 using damage parameters, elastic and inelastic strains. Figure 1 and Table 1 show the concrete behaviour and material parameters used to model deep concrete beams.

$$\varepsilon^{pl} = \varepsilon^{in} - \frac{d_c}{1-d_c}\frac{\sigma}{E_O} \tag{8}$$

$$\varepsilon^{pl} = \varepsilon^{cr} - \frac{d_c}{1-d_c}\frac{\sigma}{E_O} \tag{9}$$

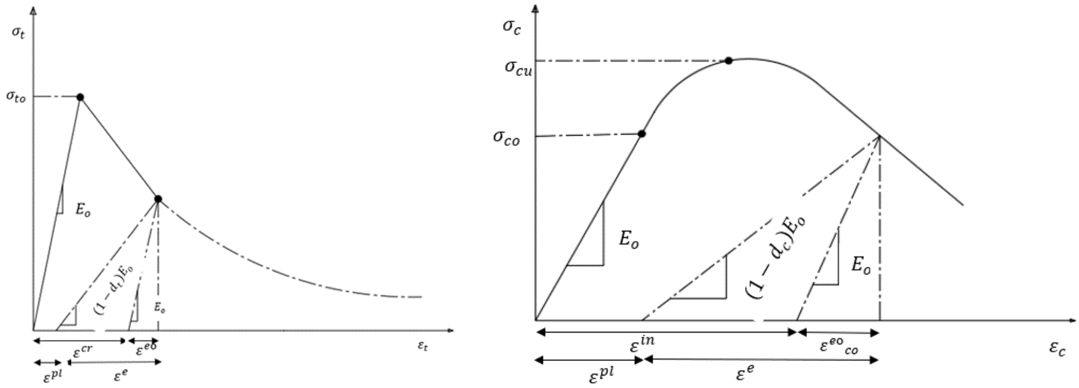

(a) Tension behaviour (b) Compressive behaviour

Figure 1. Concrete behaviour

Concrete undergoes cracks around the course aggregates that propagate to cement paste. However, due to the presence of a void in hardened concrete, the compression of such concrete will fill in the void and then increase the overall compressive strength of the concrete. Unlike ductile materials such as steel reinforcement, concrete behaves ductile only under compression. Therefore, the failure regime of concrete depends on the compaction of concrete material and its shear strength [35]. In loading concrete specimens in 3D, the hydrostatic pressure (principal stresses) is assumed to be the same in all directions in which the axis where the load is applied is always perpendicular to a deviatoric plane, as in Figures 2-a and 2-b. This pressure (hydrostatic) or dilatational stress always acts to change the volume of the material. The deviatoric pressure in that deviatoric plane corresponds to the shear capacity of the concrete specimen that distorts it without changing the volume of the materials. Therefore, the deviatoric pressure (q) and hydrostatic pressure (p) govern how concrete dilates and are measured in terms of angle. This angle is made with the flow potential function (yield failure surface) in the q-p plane, as in Figure 2-c. In this study, this angle was set to be 30º. After stress reaches the maximum failure surface, stress is then reduced to residual strength level, leading to material softening. To limit the stress beyond the tensile strength and have the same dilatancy capacity throughout the confinement, the failure surfaces have an eccentricity of 0.1. The stresses in the deviatoric plane correspond to different stress ratios, ranging from 0 to 1.0, and 1.0 means the spherical shape and no deformation has developed. This stress ratio (shape factor) is the ratio of the second stress invariant in the tensile meridian to that on the compression meridian. In this study, the default value of 0.667 was used. These second stress invariants are shear stress between T_{11} and T_{22} as shown in Figure 2 (d). In addition, the biaxial and uniaxial compression ratio was taken as 1.16.

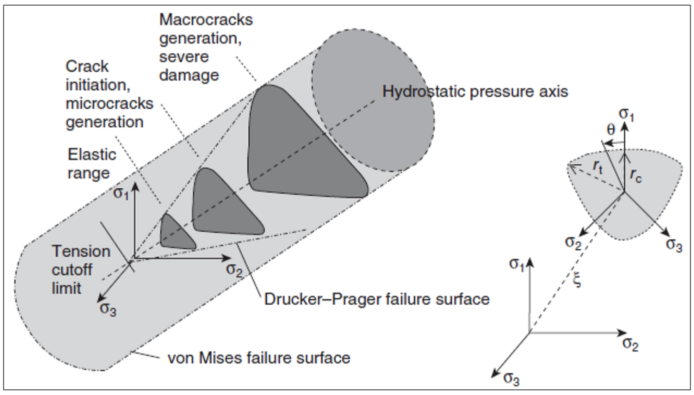

(a)

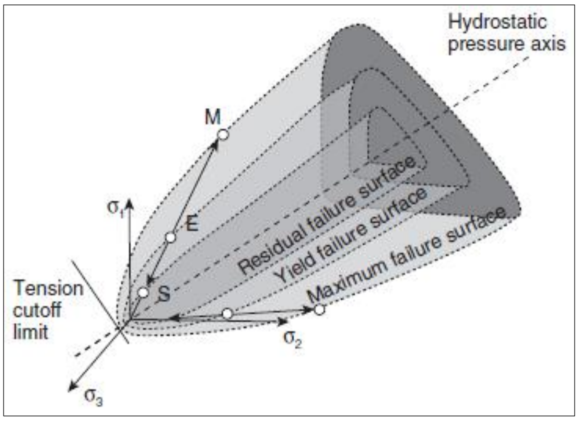

(b)

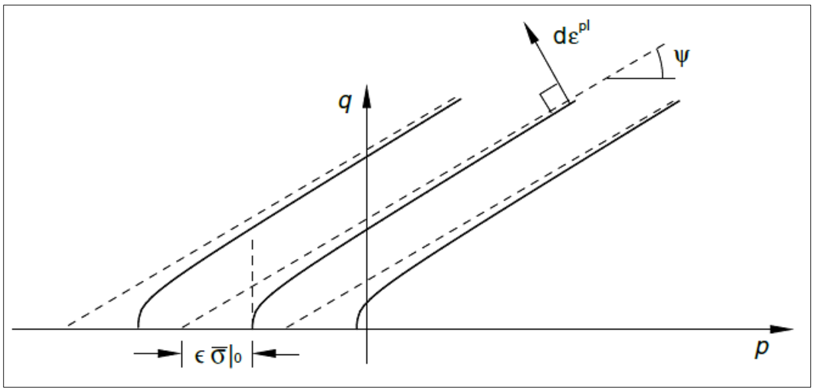

(c)

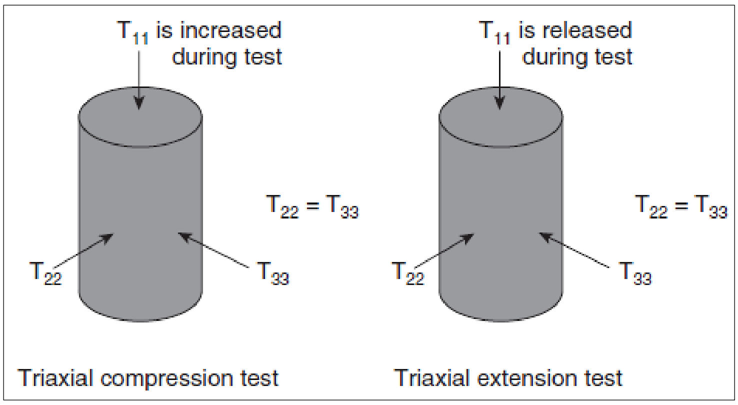

(d)

Figure 2. Material coefficients used in concrete damaged plasticity model; (a) The hydrostatic and deviatoric stress, (b) Triaxial stress state – linear approximation to consider material hardening and softening, (c) Angle of dilation in the p–q plane and (d) Compression and extension tests [32, 35, 36].

Table 1. Material parameters used in modelling of deep concrete beam

Parameter	Concrete	Steel reinforcement
Young's modulus, E_f(MPa)	33501	210000
Young's modulus, E_m(MPa)	26374	210000
Cylindrical compressive strength, f_{cm}(MPa)	51.59	-
Cylindrical compressive strength, f_{cf}(MPa)	60.6	-
Tensile strength,f_{tm}(MPa)	4.03	-
Tensile strength,f_{tf}(MPa)	4.82	-
Yield tensile strength of Y12, f_y(MPa)	-	491.95
Yield tensile strength of Y10, f_y(MPa)	-	472.64
Yield tensile strength of fibre, f_{yf}(MPa)	-	640.8
Poisson's ratio,ϑ_f	0.183	0.3
Poisson's ratio,ϑ_m	0.143	
Dilation angle	30°	-
Shape factor, K_c	0.67	-
Viscosity factor	0.00001	-
Eccentricity	0.1	-
Biaxial and uniaxial compression ratio, ${}^{\sigma_{bo}}/_{\sigma_{co}}$	1.16	-
Density, kg/m^3	2537/2536	7850

Key: *m* refers to the control mix and *f* refers to the fibre.

2.1.2. Loading and Boundary Conditions

The beam was loaded in shear in which the boundary condition was required. Steel plates were assembled at the top of the beam at an equivalent shear span-to-depth ratio of 0.8 to minimise any possible over-distortion of elements when the load is applied directly to concrete. The top surface of the steel top plates was assigned with variable displacements depending on the opening size, as shown in Table 2. To maintain the homogeneity during loading and easy-to-probe shear forces, the steel plates were also used as supports where its bottom surface was coupled using kinematic coupling to the created reference points. This coupling constrained all displacements and rotation degrees of freedom. Figure 3 shows the loading and support conditions.

Table 2. Deflections used in modelling

Beam	B_{C1}	B_{C2}	B_{C3}	B_{C4}	B_{S1}	B_{S2}	B_{S3}	B_{S4}	*B_{S1}	*B_{S2}	*B_{S3}	*B_{S4}
Deflection(mm)	1.6	2.1	1.6	5.4	3.8	2.9	3.6	1.7	2.8	4.1	3.2	5.0

Key: B_{C1}, B_{C2}, B_{C3} and B_{C4} are beams without fibres; B_{S1}, B_{S2}, B_{S3} and B_{S4} are beams with discrete distribution fibres; *B_{S1}, *B_{S2}, *B_{S3}, and *B_{S4} are beams with fibre mesh perpendicular to strut width. All sets of beams had opening sizes of 160×86, 115×120, 86×160 and 165×170 mm.

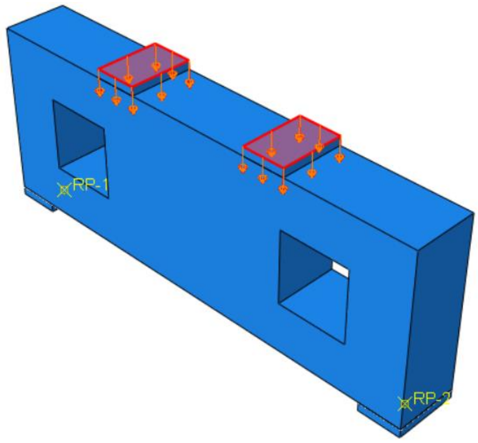

Figure 3. Loading and boundary conditions for beam B_{C4}

2.1.3. Finite Element Type, Meshing and Analysis

In the analysis step, the Abaqus/explicit solver was opted for. The solver is of benefit due to stable time increment, permitting no user interference to create stability of the model. Once the stable results are obtained, they are propagated to the next step, demanding no further checks for the stability of the analysis in that step. As far as storage is concerned, the solver does not perform iterations as for Abaqus/standard; therefore, no stiffness matrices are stored in the computer due to the embedded central difference integration scheme in it [32]. The integration scheme employs small-time increments, leading to an extended computation time but still beneficial in storage and stable time increments. The Abaqus/explicit is intentionally designed to model significant dynamic problems. However, through smoothing of the analysis step, the velocity in the model can be minimised and, therefore, less kinetic energy, as shown in Figure 4. For the Abaqus/explicit to be used in statical analysis, the kinetic energy of the entire model (ALLKE) was limited to 5% of the total internal energy of the whole model (ALLIE).

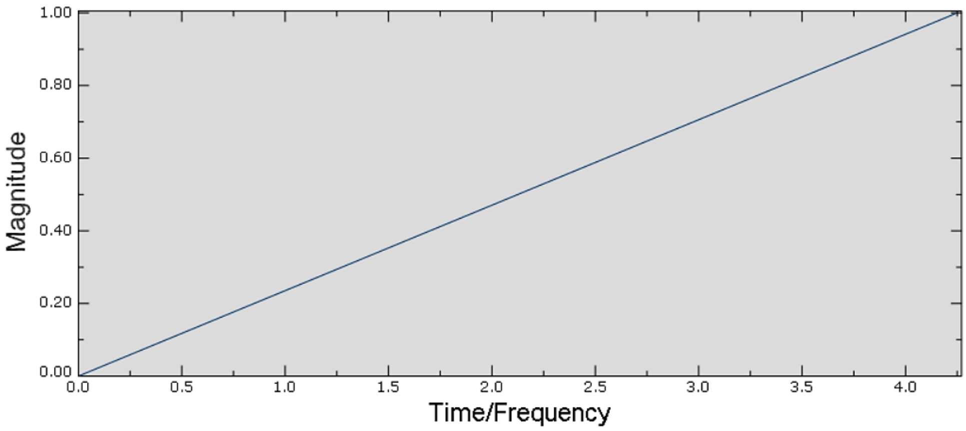

(a) Unsmoothed step amplitude (dynamic analysis)

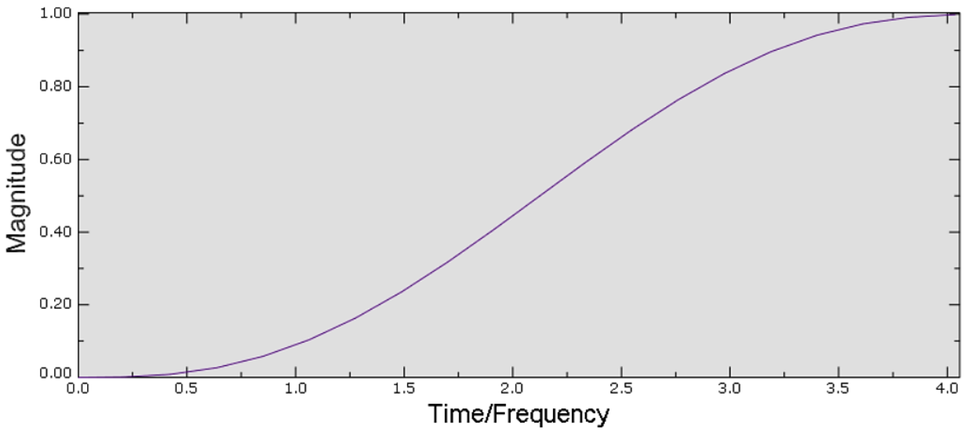

(b) Smoothed step amplitude (quasi-static analysis)

Figure 4. Smoothing step in explicit solver for quasi-static analysis on B_{C3}

To limit any unnecessary displacement of steel reinforcements in the beam before loading, the embedded constraint was used to create the interaction mechanism in the composite. This embedded constraint utilises the finite element called the truss-in-solid embedded element. The concrete beam was the hosting region, and all steel reinforcement and the fibre mesh were embedded regions. Only translational nodes in the embedded elements were eliminated from the embedded nodes. These nodes were constrained to the interpolated values of the corresponding degrees of freedom of the host element [37]. Concrete and steel fibres/mesh were modelled in discretisation using a solid homogenous element called hexahedron, C3D8 and T2D3 elements, respectively. All elements had the same mesh size of 20 mm, so any variations of meshes were avoided since the small mesh sizes controlled the time increment in Abaqus/explicit. The meshed beam and element type are shown in Figure 5.

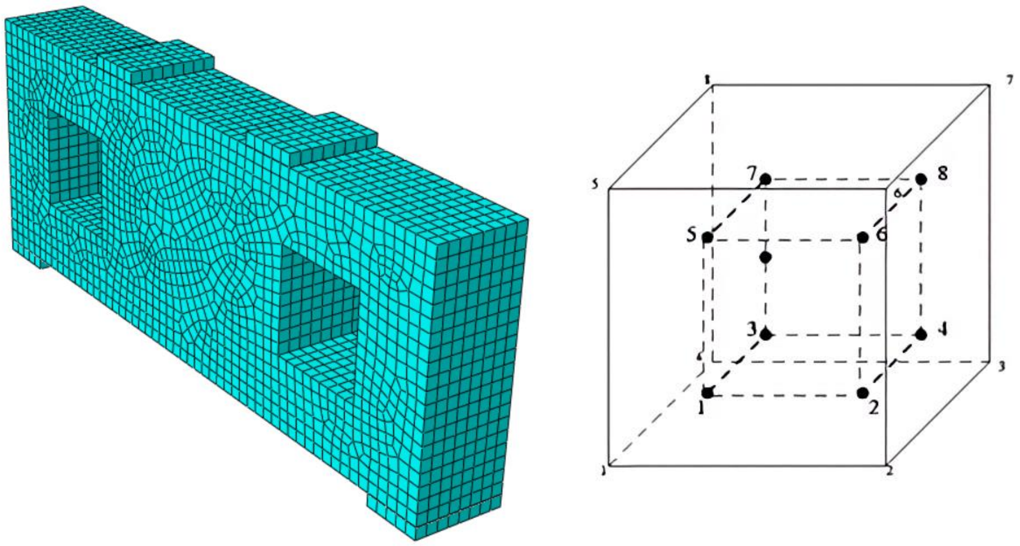

(a) 20 mm mesh size of C3D8 (b) C3D8 element with 2×2×2 fully integration scheme

Figure 5. Meshing and finite element type

2.2. Testing of Deep Concrete Beam

The deep beam with 150×400×1100 mm was used in the study by Augustino et al. [1]. The beam dimension was designed based on the specifications described in ACI 318-19 [29] and EN 1992-1-1 [38]. Table 3 shows the type of beams used and the corresponding transverse openings. Figure 6 presents the loading setup, reinforcement configurations, possible crack pattern, and compressive struts. The opening in the deep concrete beam was used to assess the reduction of shear resistance. Therefore, the deep beam had a shear span and an effective depth of 300 and 376 mm, respectively. The beam with fibres had concrete with 50 mm fibre length and 0.5% fibre content (SFRC50-0.5).

Table 3. Beam type and opening sizes

Group of beams	Beams	Transverse Opening (x×h), mm	Depth of the beam, D, mm
B_C	B_{C1}	160×86	400
	B_{C2}	115×120	
	B_{C3}	86×160	
	B_{C4}	165×170	
B_S	B_{S1}	160×86	400
	B_{S2}	115×120	
	B_{S3}	86×160	
	B_{S4}	165×170	
$^*B_S$	$^*B_{S1}$	160×86	400
	$^*B_{S2}$	115×120	
	$^*B_{S3}$	86×160	
	$^*B_{S4}$	165×170	

Key: ***c*** is for control; ***s*** is with 50 mm fibre length; ****s*** with fibre and fibre mesh.

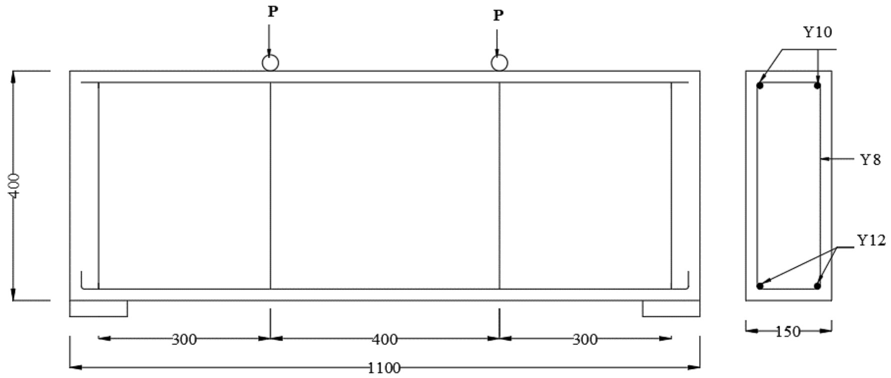

(a)

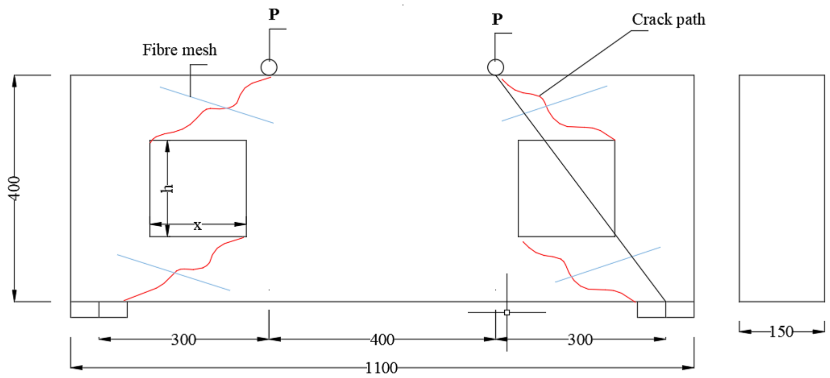

(b)

Figure 6. Deep concrete beam test setup (a) steel reinforcement detail and (b) location of fibre mesh and crack path

2.3. Statistical Analysis

Statistical analysis was deployed to assess the significance of the predicted shear resistance. These statistical measures for two independent variables were the performance factor (PF), Coefficient of variation (COV) and Mean absolute error (MAE) [39, 40]. The performance factor is the ratio between the experimental and shear resistance in the available model, as shown in Equation 10.

$$PF = \frac{V_{exp}}{V_{cal}} \tag{10}$$

where; V_{exp} is an experimental shear resistance in kN and V_{cal} is the predicted shear resistance using available shear analytical models in kN.

The COV was used to measure the closeness of shear resistance between independent sets of data, and the smaller COV indicates the minimised scatter in results. COV uses the performance factor of two data sets to evaluate their correlation. Generally, COV suggests the accuracy of results and is defined using Equation 11.

$$COV = \frac{Sample\ deviation(\sigma)}{Mean(\mu)} \tag{11}$$

MAE specifies an error between the experimental shear resistance and that from the predicted models. It is the mean of the difference between measured and predicted values expressed as percentages of the experimental value, as in Equation 12.

$$MAE = \frac{1}{n}\sum\frac{V_{exp}-V_{cal}}{V_{exp}} \tag{12}$$

Here, *n* is the number of test specimens. The null and alternative hypotheses were formulated in this methodology to assess the significant difference between measured and FE model shear values. The null hypothesis was that the mean shear values were the same for both experimental and finite element model shear capacities. A t-test was used to assess these hypotheses. The smaller the t-stat, the closer the sets of independent shear capacities are; hence, the null hypothesis was accepted and otherwise rejected. The following flow chart summarises the method chapter (Figure 7).

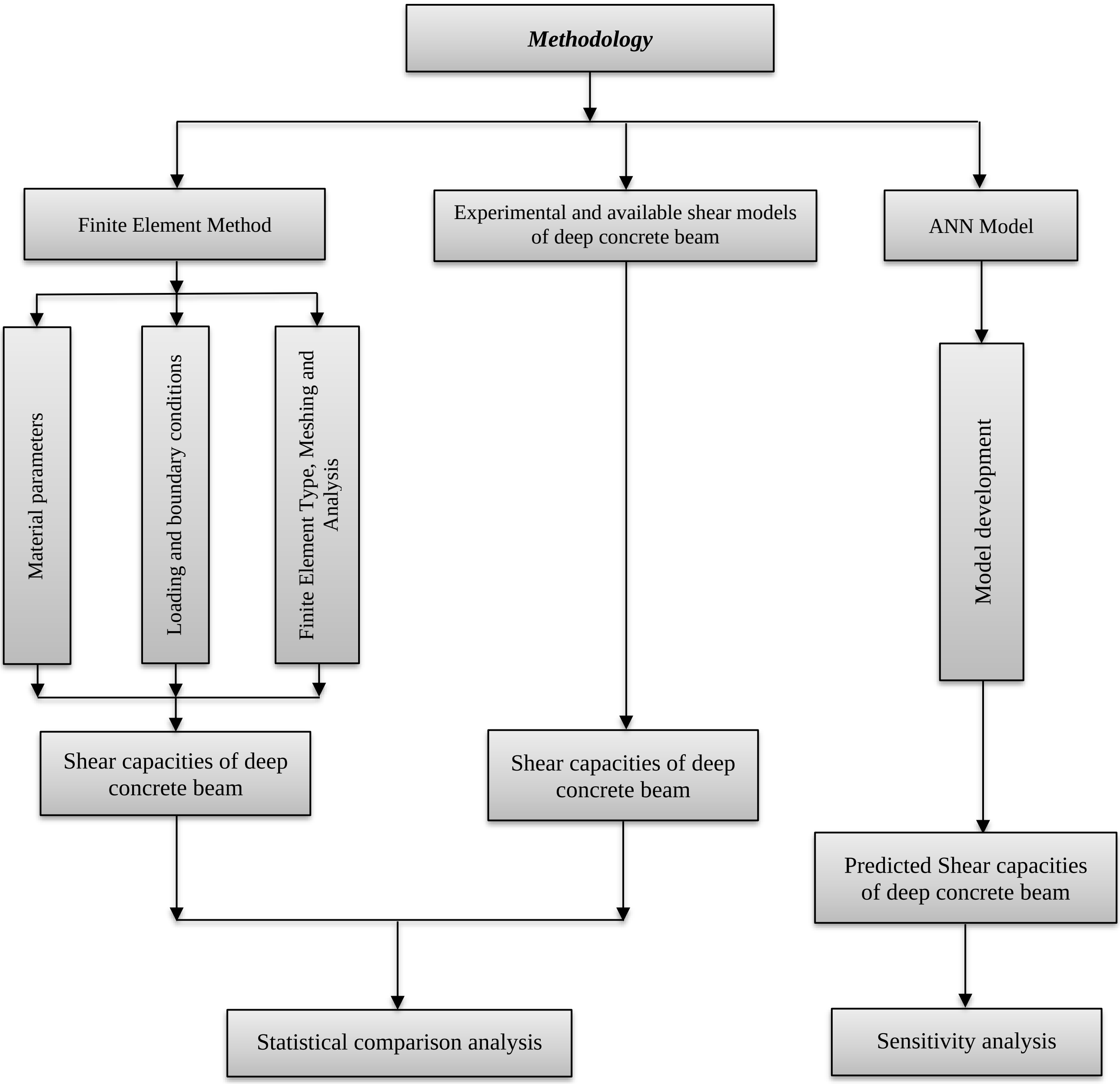

Figure 7. Flowchart of the methodology

3. Results and Discussion

3.1. Concrete Damage Plasticity Constitutive Models

The results in Figure 8 are the plots of the concrete constitutive models and the damage evolution of concrete. Concrete had a mean cylindrical compressive strength of 51.59 MPa and 60.06 MPa for control beams and beams with fibres, respectively. Up to the failure of the concrete cylinder, the model was established using experimental results. From the ultimate compressive stress of the curve, the descending part of the curve was based on the models [41–43]. The results showed that the fibres exhibit a high post-cracking behaviour due to strain hardening from the compressive stress of 48.41 MPa. The experimental results for concrete tensile strength and Young’s modulus were 4.82 MPa and 33501 MPa, respectively. The constitutive models in Rai [34] were used to develop the tension-softening part of the stress-strain curve with peak tensile strains of 0.000144 and 0.00015 for steel fibre-reinforced concrete with 50 mm fibre length and 0.5 fibre content (SFRC50-0.5) and control mix (CM), respectively. The CM cylinder was split entirely into halves, while the SFRC50-05 cylinders resisted the propagation of the crack. Therefore, the force to cause the same strains in the curves was greater for fibre-reinforced concrete than an unreinforced matrix due to the individual tension stiffening of fibres in concrete.

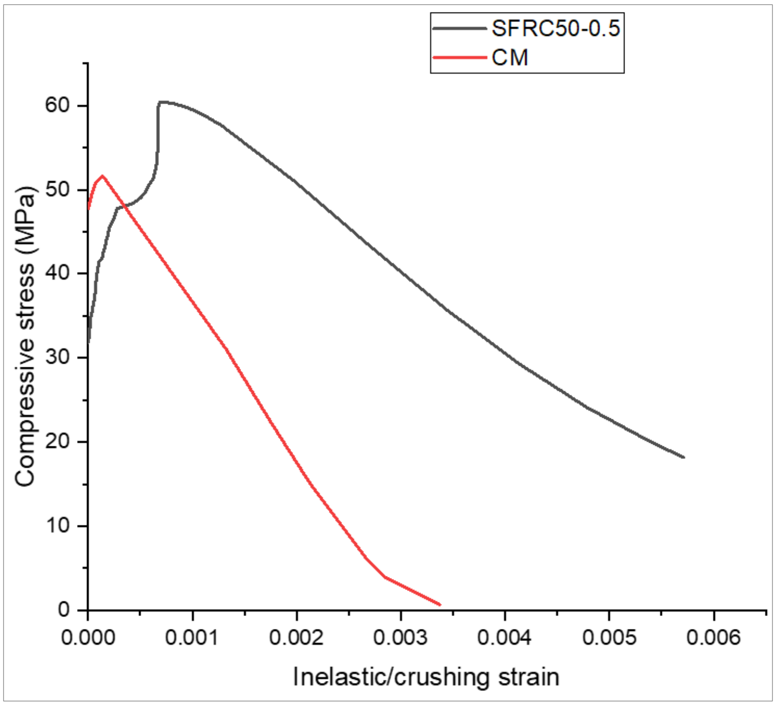

Compressive damage model

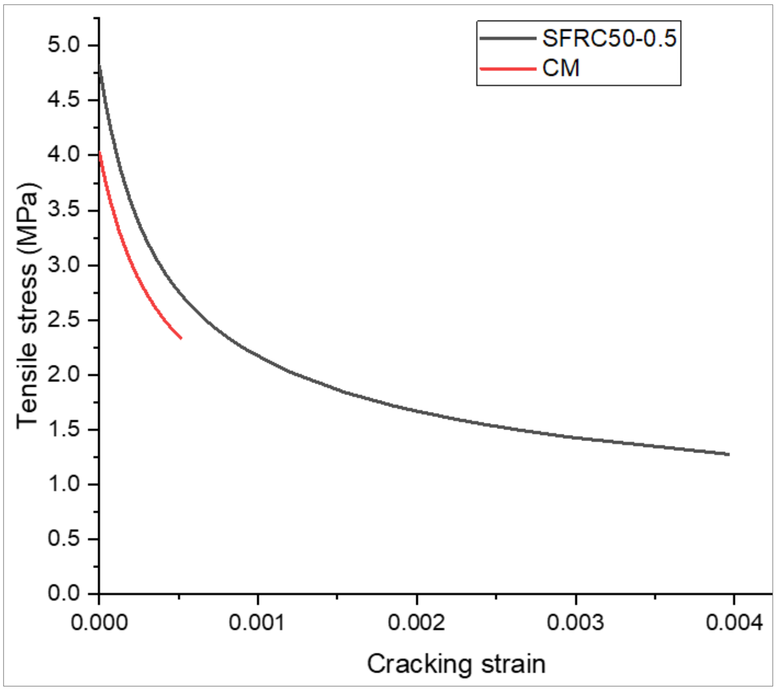

Tensile damage model

Figure 8. Damage evolution of concrete

3.2. Failure Modes of Deep Concrete Beams

The results in Figures 9 and 10 present the failure modes, DamageT and SDEG in control beams and beams with fibres, respectively. The results show a high damage parameter in the beam with a transverse opening of 165×170 mm, indicating a slight remaining stiffness in the matrix. In Abaqus, the control beam showed a broad band of damage compared to the beams with fibres, which suggests the early failure of control beams. The fibre-reinforced beams (B_{S2} and B_{S1}) showed higher resistance to stiffness degradation than the other beams. These FE failure modes conform to findings by Hussein & Abbas [4] and Ibrahim et al. [7] and agree with experimental failure patterns as reported early in Augustino et al. [1]. In addition to stress paths above the openings, beams with transverse openings 86×160 mm without fibres, all beams with 165×170 mm and beams with meshes showed a weak lower load path that resulted in sudden strut failure. This weak load path is mainly affected by fibres and the opening size. For beams with fibres and depth less than 4D, there is no formation of lower and upper load paths.

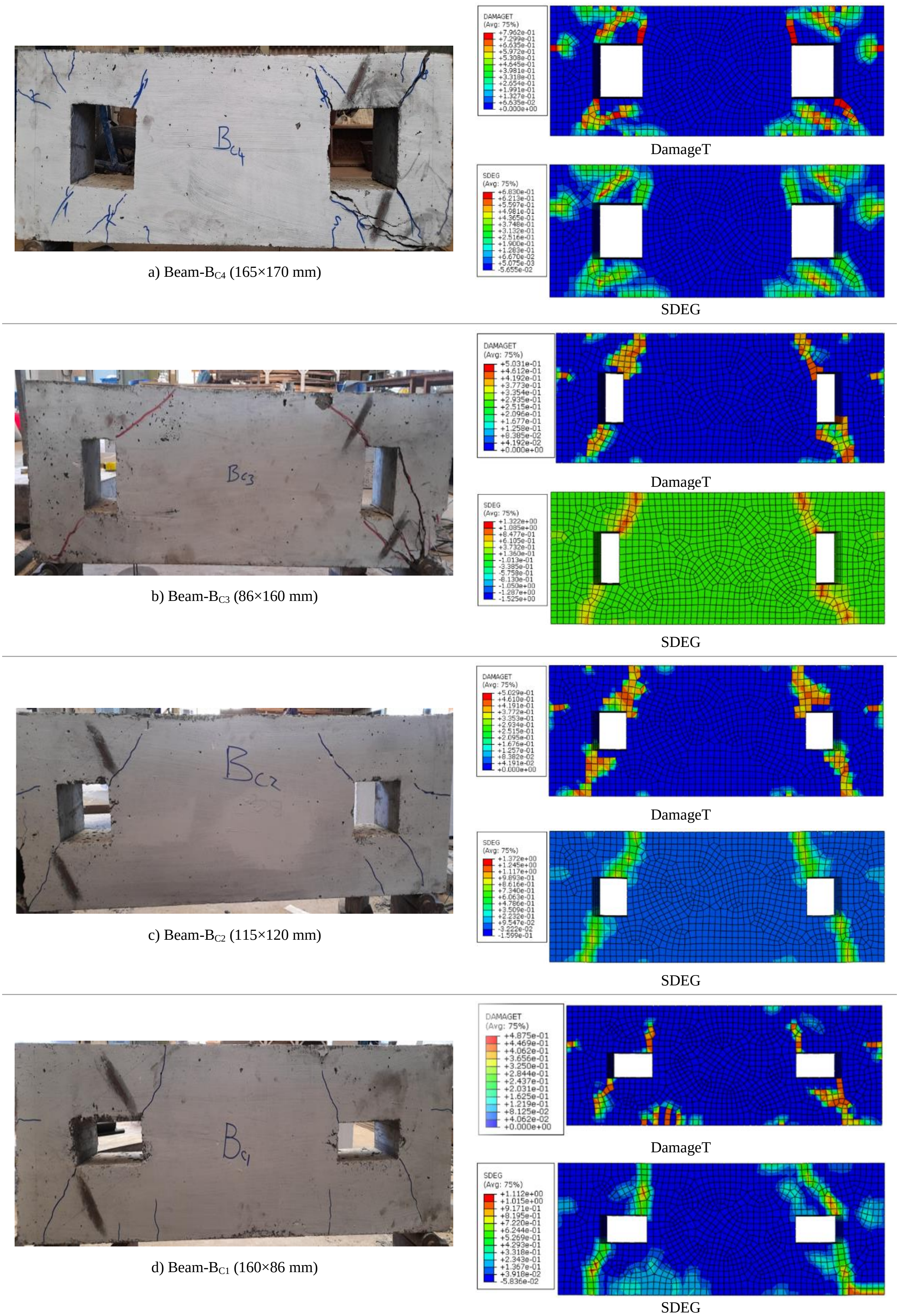

a) Beam-B_{C4} (165×170 mm)

b) Beam-B_{C3} (86×160 mm)

c) Beam-B_{C2} (115×120 mm)

d) Beam-B_{C1} (160×86 mm)

Figure 9. Failure modes, DamageT and SDEG in control beams

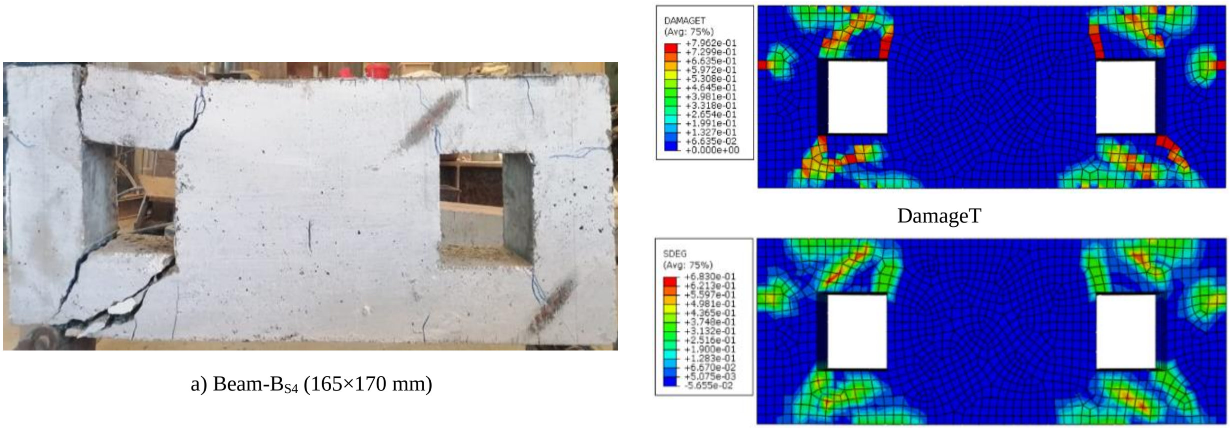

a) Beam-B_{S4} (165×170 mm)

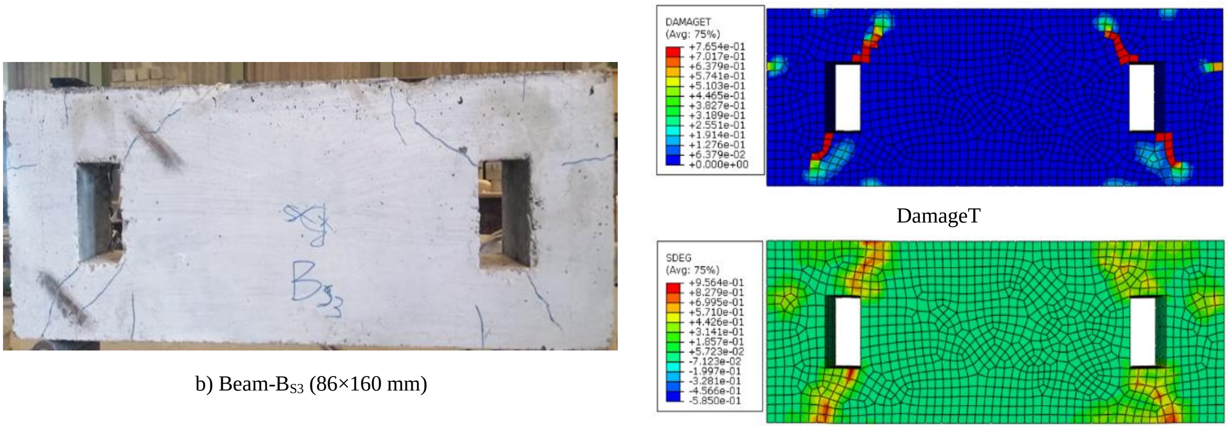

b) Beam-B_{S3} (86×160 mm)

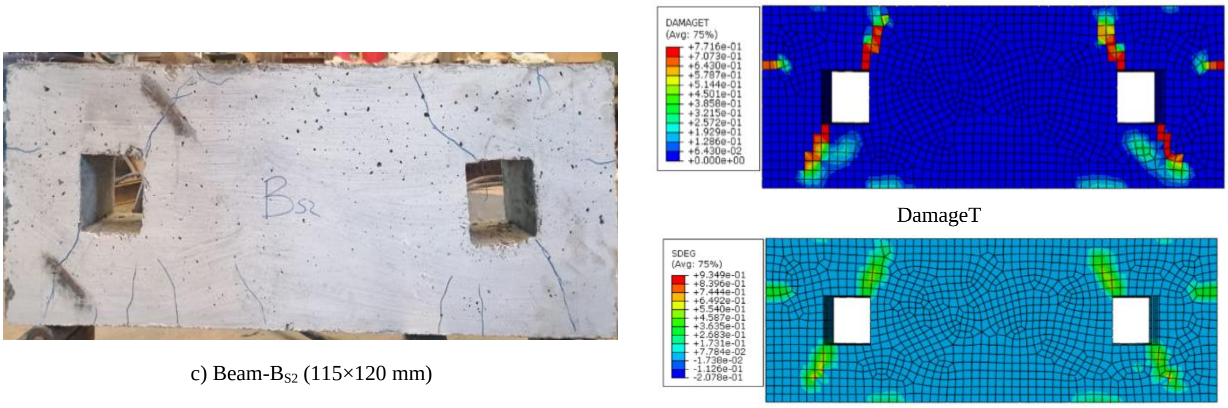

c) Beam-B_{S2} (115×120 mm)

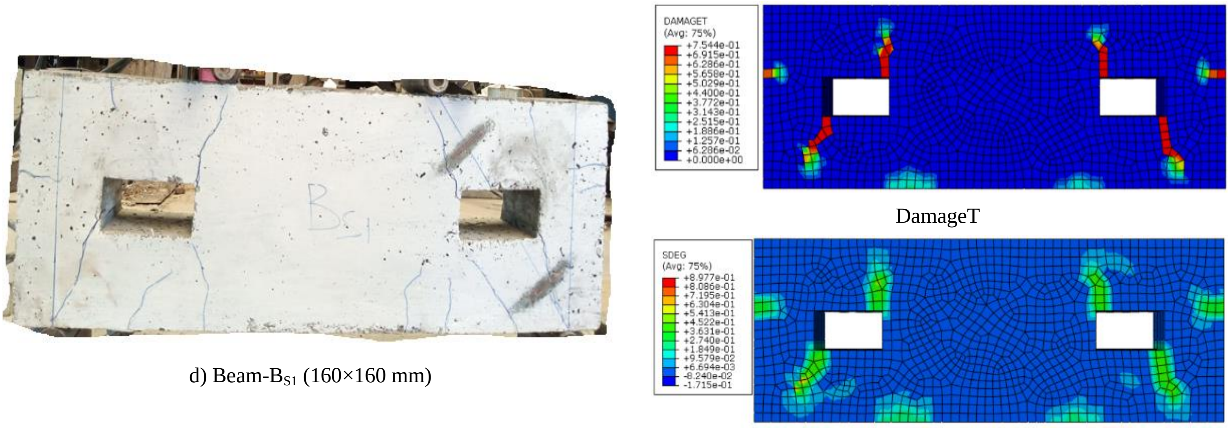

d) Beam-B_{S1} (160×160 mm)

Figure 10. Failure modes, DamageT and SDEG in beams with fibres

3.3. Effect Of Opening and Fibre on Stress Distribution along the Depth of the Beam

Results in Figure 11 present the stress distribution along the depth of the beam. The results show that the addition of fibres in the beam lowered the neutral axis from the bottom chord of the beam, leading to a high compressive stress zone. This resulted in a high shear resistance of fibre-reinforced beams compared to beams without fibres. For example, B_{S2} had a 15.8% less neutral axis compared to B_{C2}. The trend agrees with Lantsoght [44] that fibres in concrete have limited improvement in compressive strength compared to when fibres are subjected to tensile loads. For shear stresses to be generated at the fibre-concrete interface, fibres are required to be subjected to tensile cracks rather than compressive cracks. Therefore, in addition to conventional tensile steel reinforcements, fibres in the tension chord of the beam contribute to overall tensile forces through tension stiffening. These forces need to balance with compressive forces due to the concrete above the neutral axis. Since fibres increase tensile forces, a small lever arm is required to balance the neutral axis with a counteracting moment in the compression zone. This scenario resulted in a significant compression zone depth compared to the tensile zone. The significant depth in the compression zone resulted in a high compressive stress of 80% at the top chord of the beam, $B_{S2,}$ compared to the beam without fibres, B_{C2}. The beam with and without fibres with an opening height of 0.43D had a less neutral axis of 17.1% and 39.5% compared to an opening with a height of 0.22D, respectively. However, due to the high reduction in adequate depth and interruption of the interior strut, the less neutral axis had less effect on the shear resistance of the deep concrete beam. Furthermore, results show that beams with the opening with the same area (B_{C1}, B_{C2}, B_{C3}) at mid-depth in the shear zone had the same compressive stress of 0.6 MPa compared to a tensile stress of 0.34 MPa for a beam with an opening of size 165×170 mm, B_{C4}. From the mid-depth of the beam, stress at the shear span increases towards the tensile behaviour as the opening length increases. This phenomenon results in the cracking of the inner upper corner of the opening. However, beams B_{C3} and B_{C4} failed due to stress concentration at the remaining depth of the opening above it, which resulted from the rotation of concrete parts around the opening.

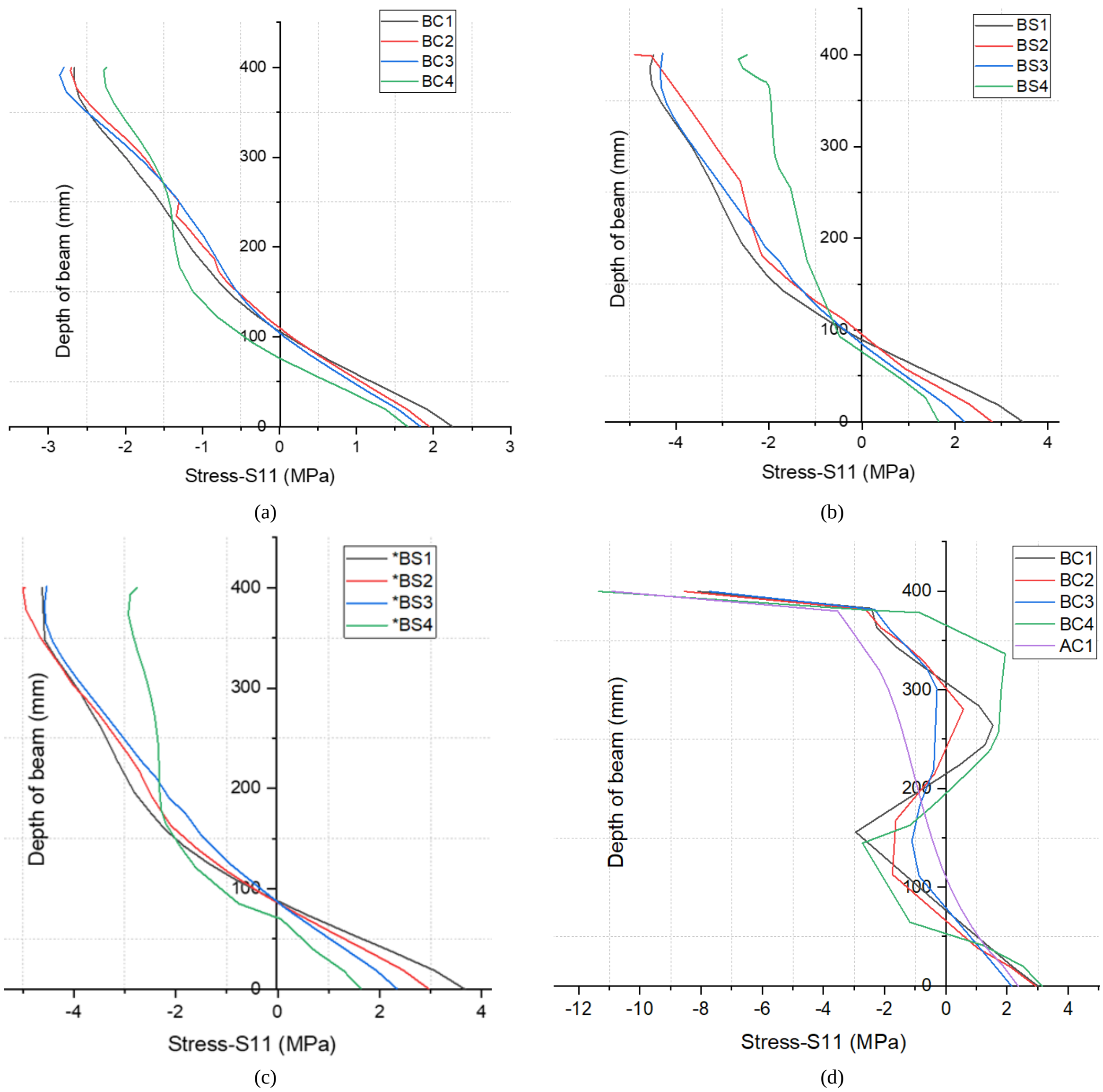

Figure 11. Stress distribution along the depth of the beam;(a) At the mid-span; control beams, (b) At the mid-span; beams with fibres, (c) At the mid-span; beams with fibres and mesh and (d) At 300 mm from the centre of the support-control beam

3.4. Strain Distribution Along Steel Reinforcements

3.4.1. Along the Top Steel Reinforcement

Figures 12 and 13 show the contour of strain distribution along the steel reinforcements and the strain distribution along the top steel reinforcement, respectively. The results show that the control beam with a transverse opening of 165×170 mm had compressive strain at mid boundary strut of 16.2, 26.6, and 17.9% less than beams with a transverse opening of 160×86, 115×120, and 86×160 mm, respectively. The results also show that the beam with fibres and a transverse opening of 165×170 mm had compressive strain at the mid of the boundary strut of 70.5, 85.6, and 62.9% less than the beams with the transverse opening of 160×86, 115×120, and 86×160 mm, respectively. Furthermore, the results show that beams with fibre mesh and a transverse opening of 165×170 mm had compressive strain at mid boundary strut of 65.9, 74.1, and 58.9% less than beams with a transverse opening of 160×86, 115×120, and 86×160 mm, respectively. The strain distribution in the top reinforcement showed less compressive behaviour for a large opening due to induced tensile stresses. The compression steel reinforcement in the boundary strut had high compressive strains for the beam with a square opening due to the stiffness contribution of the remaining depth of concrete above the opening and less interruption of strut width. These findings support [29] the hypothesis that top reinforcement in the length of the boundary strut contributes to the shear resistance of the deep concrete beam. Although the addition of fibres increases the compression behaviour of the boundary strut, it does not limit the concentration of tensile stress on the top bar in the region at the upper outer corner of the opening as depth increases. This increase in tensile strain in these regions for all openings leads to the rotation of the upper part of the opening, hence cracking of the opening at the top of the beam [45]. Therefore, an increase in the depth of the opening causes the compressive steel reinforcement to have a minimal contribution to shear transfer, as it fails under relatively less compression in the beam's boundary strut.

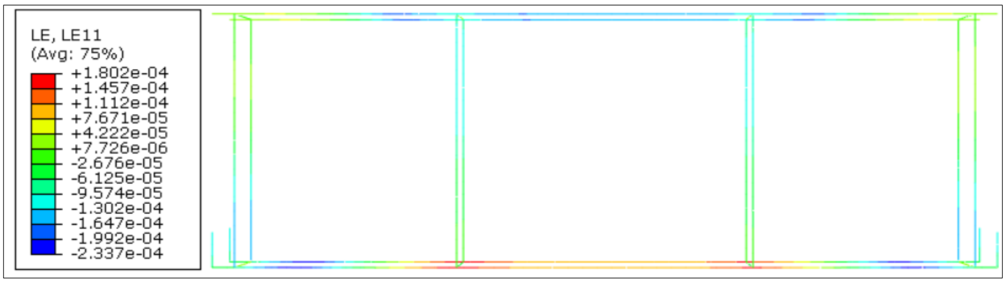

B_{S1}

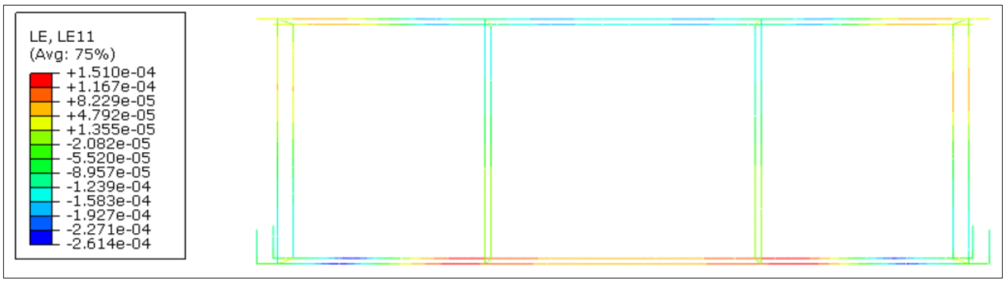

B_{S2}

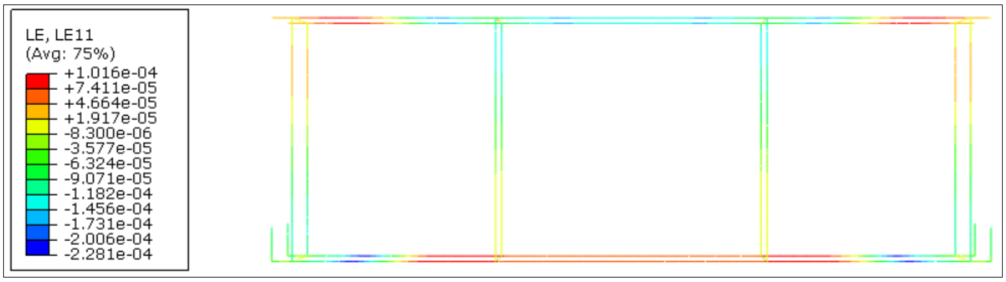

B_{S3}

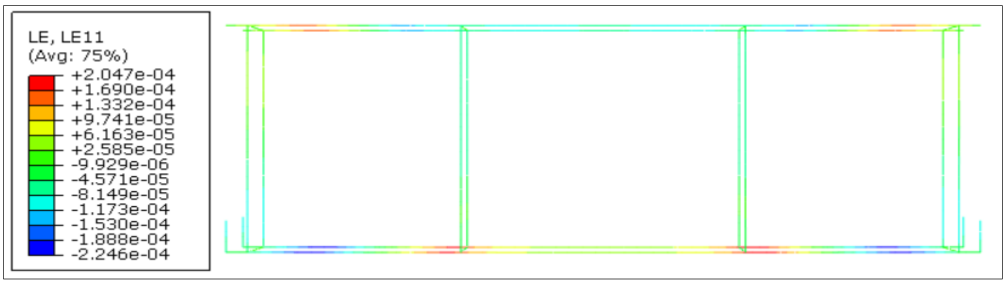

B_{S4}

Figure 12. Contour of strain distribution along the steel reinforcements

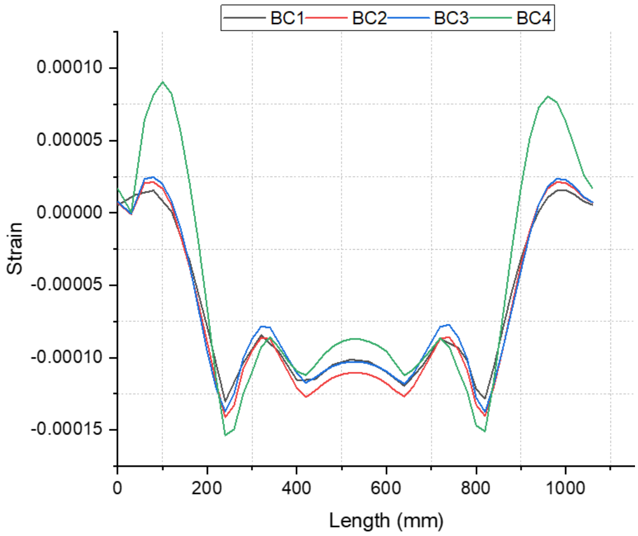

(a)

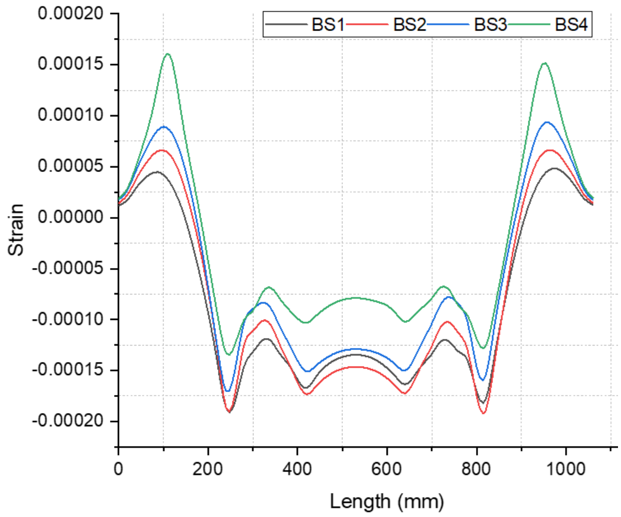

(b)

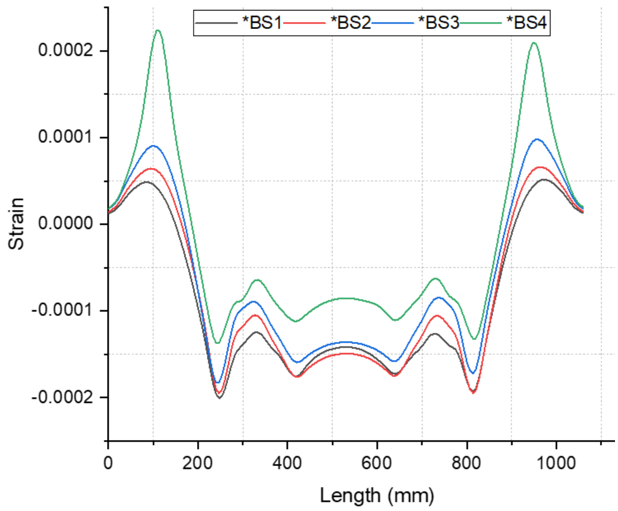

(c)

Figure 13. Strain distribution along the top steel reinforcement. (a) Beams without fibres, (b) Beams with fibres and (c) Beams with fibres and mesh

3.4.2. Along Bottom Steel Reinforcement

Results in Figure 14 present the strain distribution along the bottom steel reinforcement. The results show that the control beam with a transverse opening of 160×86 mm was stiffer in the middle part, with strain in the main bar of 6.7, 23.7, and 40% higher than the beams with a transverse opening of 115×120, 86×160, and 165×170 mm, respectively.

The results also show that the beam with fibres and a transverse opening of 160×86 mm had a mid-strain of 10.3, 62.3, and 115% higher than the beam with a transverse opening of 115×120, 86×160, and 165×170 mm, respectively. Furthermore, the results show that the beam with fibre mesh and a transverse opening of 160x86 mm had a mid-strain of 23.6, 56.1, and 134% higher than the beam with a transverse opening of 115×120, 86×160, and 165×170 mm, respectively. These findings are consistent with Alsaeq [46] and Mohamed et al. [47] that the horizontal steel bar redistributes stress in the middle part of the beam, in which the presence of a narrow opening could improve flexural rigidity compared to a beam with a high opening depth. The remaining area above the opening increases the flexural stiffness, leading the beam to withstand more loads. These loads in the section create stresses at the midpoint of the beam, resulting in high strains along the main steel bar. The results also show that the beam with a transverse opening of 115×120 mm and fibres in the shear zone had high compressive strain along the main steel reinforcement. These agree with a previous finding [48] that interruption of the strut width significantly affects the shear resistance of the deep concrete beam. The opening 115×120 mm had less interception of strut width compared to 160×86 mm, resulting in high compressive strain in the region. It was further observed that openings in the shear zone of the beam create strain variation from tensile to compression strains along the main steel reinforcement at the inner and outer corners of the opening, respectively. These tensile strains in the inner corner of the opening caused an abrupt failure, particularly in the control beams and beam with mesh, which contributes to the formation of dowel action in the main bar [3]. In addition, as the length of the opening increases, the strains at the joint of the bottom steel bar and the stirrup increase. This is associated with nonlinear stress concentration around the opening as the load is transferred to the support through the lower load path near the stirrup. An increase in an opening length creates a D-region that creates more nonlinear stress concentration and paths adjacent to the stirrup, causing cracks at the corners of the opening [45, 49]. This concludes the high tensile strains at the joint between the tensile steel bar and stirrup for the beam with a transverse opening of 165×170 mm compared to 86×160 mm.

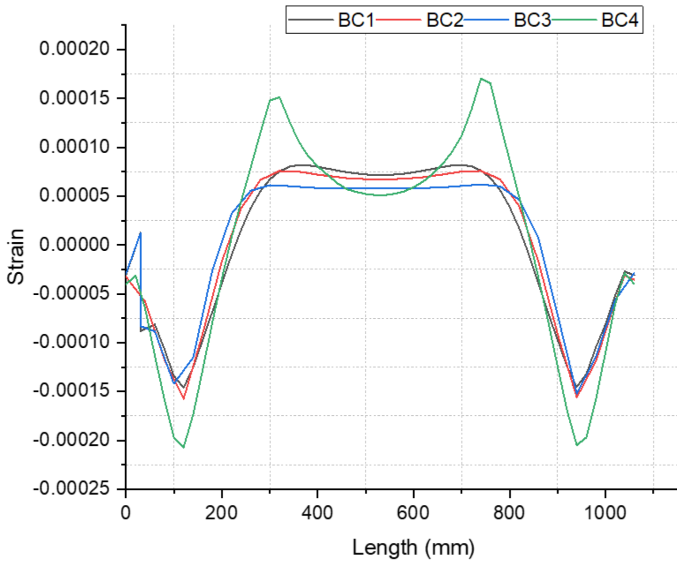

(a)

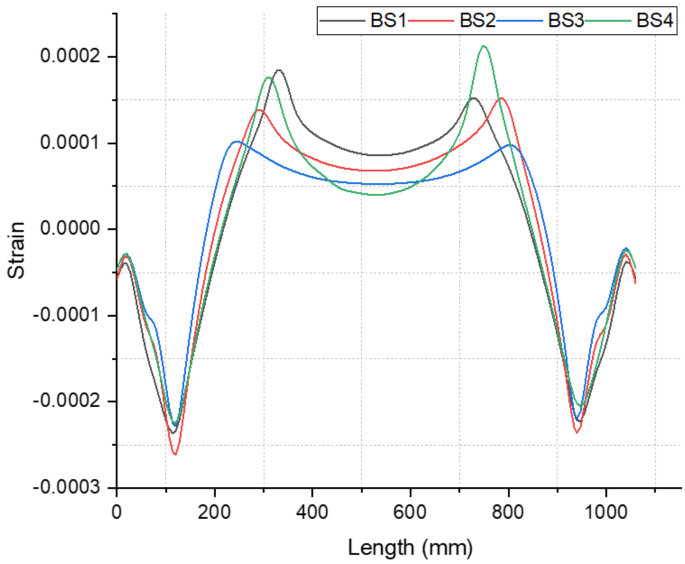

(b)

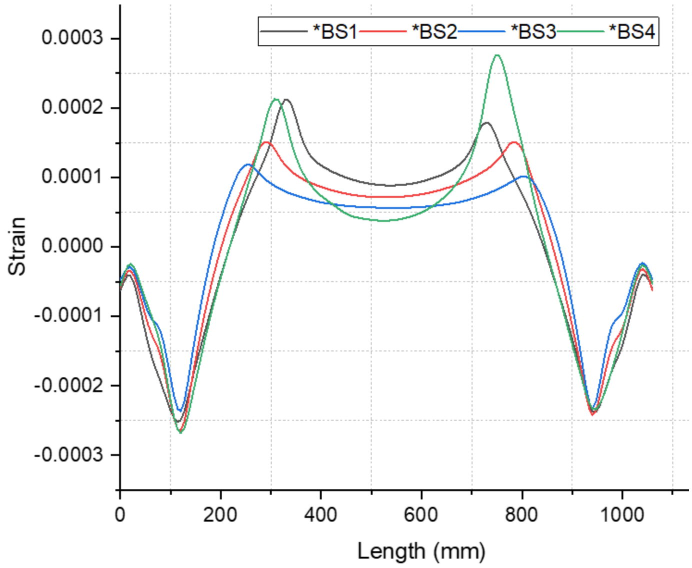

(c)

Figure 14. Strain distribution along the bottom steel reinforcement. (a), Beams without fibres (b) Beams with fibres and (c) Beams with fibres and mesh

3.5. Comparison of the FE Model and Experimental Shear Resistance

3.5.1. Deep concrete Beams with Transverse Openings and Without Fibres

The results in Figure 15 and Table 4 compare the performance of the finite element model and measured shear resistance for control beams. The measured shear resistance for beams B_{C1}, B_{C2}, B_{C3} and B_{C4} were 2.9, 3.0, 5.7 and 4.3% less than FEM shear resistance, respectively. This indicates a slight variation between these two sets of data. The results show that measured and finite element model shear resistance had a coefficient of variation and mean absolute error of 1.38 and 4.14%. These results indicate that the finite element model and measured shear capacities are close to each other. The small coefficient of variation and mean absolute error indicate the precision of results and the minimised amount of scatter. The data sets were assessed using a t-test, considering the variances' difference. Results show that the t-value was 1.1 less than the t-critical of 1.94 and the mean of Vexp/Vcal of 0.96, indicating that there isn't a significant difference in mean shear capacities between these two data sets. The correlation between measured and FEM shear resistance was good, with the R^2 of 0.9492.

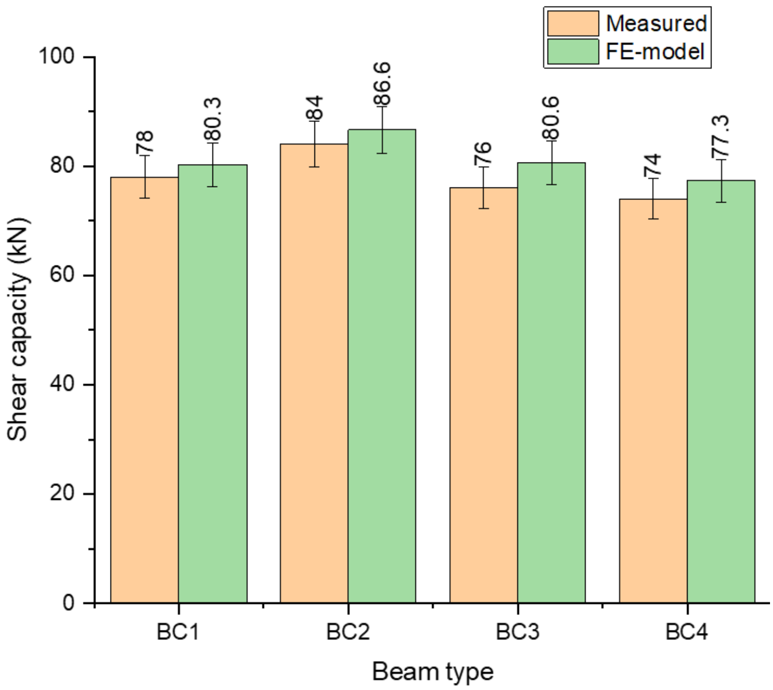

Figure 15. comparison of the performance of the finite element model and measured shear resistance for control beams

Table 4. The comparison of the statistical performance of the shear resistance of a deep concrete beam without fibres

Beam type	FE model, VFEM (kN)	Measured Vexp (kN)	Vexp/ VFEM
BC1	80.3	78	0.971
BC2	86.6	84	0.97
BC3	80.6	76	0.943
BC4	77.3	74	0.957
Mean			0.96
std			0.013
COV, %			1.38
MAE, %	4.139		
t-stat	1.1		
R^2	0.9492		

3.5.2. Deep Concrete Beams with Transverse Openings and Fibres

The results in Figure 16 and Table 5 show the comparison of the performance of the finite element model and measured shear resistance for beams with fibres. The measured shear resistance for beams BS1, BS2 and BS3 were 2.4, 3.6 and 6.7% less than FEM shear resistance, respectively. Beam, BS4 had a 7.1% measured shear resistance higher than those from the finite element model. The results also show that the measured and finite element model shear capacities had a coefficient of variation and mean absolute error of 6.1 and 5.01%. The small coefficient of variation and mean absolute error imply the proximity of results under consideration. The mean shear resistance between two sets of data, the FE model and measured, was assessed using a t-test. Results show that the t-value was 0.993 less than the t-critical of 1.943, and the mean of Vexp/Vcal of 0.986 indicates that there isn't a significant difference in mean shear capacities between these two data sets. The correlation between measured and FEM shear resistance was strong, with the R^2 of 0.974.

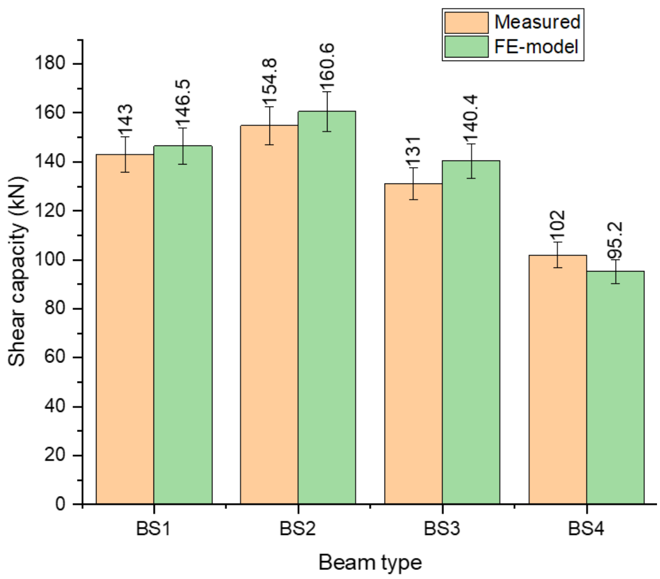

Figure 16. Comparison of performance of the developed mathematical shear model, finite element model and measured data for beams with fibres

Table 5. The comparison of the statistical performance of the shear resistance of a deep concrete beam with fibres

Beam type	FE model, V_{FEM} (kN)	Measured V_{exp} (kN)	V_{exp}/ V_{FEM}
B_{S1}	146.5	143	0.976
B_{S2}	160.6	154.8	0.964
B_{S3}	140.4	131	0.933
B_{S4}	95.2	102	1.071
Mean			0.986
std			0.06
COV, %			6.1
MAE, %	5.01		
t-stat	0.992		
R^2	0.974		

3.5.3. Deep Concrete Beams with Transverse Opening and Fibre Mesh

The results in Figure 17 and Table 6 show the comparison of the performance of the finite element model and measured data for beams with fibre mesh. The results show that the measured shear resistance for beams $*B_{S1}$, $*B_{S2}$ and $*B_{S3}$ and $*B_{S4}$ were 18.2, 18.5, 15 and 16.5% less than FEM shear resistance, respectively. The results of shear capacities between the measured and developed models seem very close; however, the segregation of fibres in the shear zone during the casting process of beams with mesh might have resulted in small measured shear capacities. These findings line with Li [50] that the vibration of fibre-reinforced concrete to achieve homogeneity of ingredients might cause the segregation of fibres, leaving the core part unreinforced. Since high-strength concrete is brittle [24], this segregation of fibres resulted in less shear resistance for the beam with fibre mesh. The results show that the measured and finite element model shear resistance had a coefficient of variation and mean absolute error of 1.95 and 20.6%. The results also show that the shear capacities between the FE model and the measured had an error of 20.6% and a t-value of 1.59, close to the t-critical of 1.943 due to low measured shear resistance with the reason mentioned above. However, the statistical test is within the acceptable range. Besides the segregation of fibres that affected shear resistance, the correlation between measured and FEM shear resistance was strong, with the R^2 of 0.9868.

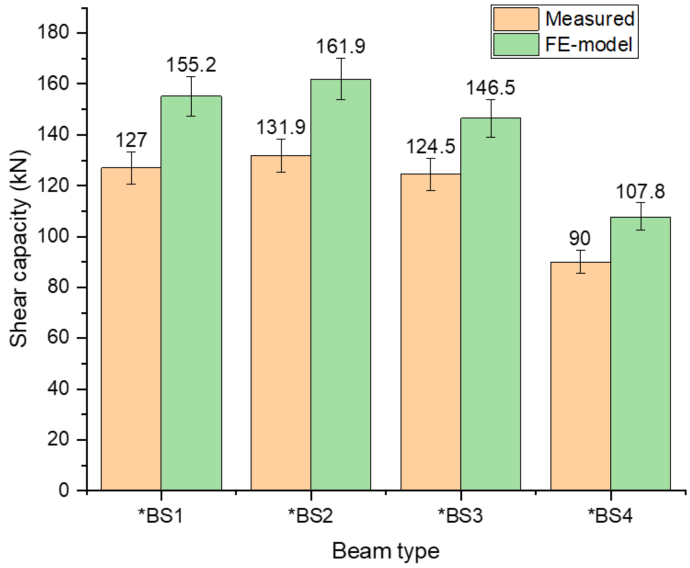

Figure 17. Comparison of performance of the developed mathematical shear model, finite element model and measured data for beams with fibres and fibre mesh

Table 6. The comparison of the statistical performance of shear resistance of the deep concrete beam with fibre mesh

Beam type	FE model, V_{FEM} (kN)	Measured V_{exp} (kN)	V_{exp}/V_{FEM}
$*B_{S1}$	155.2	127	0.818
$*B_{S2}$	161.9	131.9	0.815
$*B_{S3}$	146.5	124.5	0.85
$*B_{S4}$	107.8	90	0.83
Mean			0.829
std			0.016
COV, %			1.95
MAE, %	20.6		
t-stat		1.59	
R^2		0.9868	

3.6. Artificial Neural Network (ANN) Model Formulation

The ANN technique is used in different ways, from social sciences to engineering. The ANN model in this study was formulated using the ANN toolbox provided in MATLAB [14] to predict the effect of opening on the shear performance of reinforced deep concrete beams with and without steel fibres. A total of 56 data, i.e., experimental, analytical and FEM, were used to train, validate and test the model. As for any other model, the selection of inputs is paramount as it dictates the final prediction. The shear resistance of deep concrete beams with transverse openings depends mainly on the effect of the opening [1, 46], compressive strength, dowel action, stirrup reinforcement, aggregate interlock and, to some extent, compressive reinforcement as in ACI 318-19 [29]. The aggregate interlock in concrete with fibre has less effect, forming a base for not selecting the stirrup effect as a variable in this prediction [3, 51, 52]. The input variables which have a substantial effect on the shear performance of deep concrete beams with transverse opening were considered as follows; orientation factor of traverse opening (x_1), compressive strength for concrete with and without fibres (x_2) as in Augustino et al. [24] and the ratio of the opening area to the shear area (x_3) as shown in Equations 13 to 15, respectively.

$$x_1 = \varphi = 1 - average\ (x/a\ \ and\ \ h/d) \tag{13}$$

$$x_2 = f_{cu} \tag{14}$$

$$x_3 = {}^{A_o}/_{A_s} \tag{15}$$

In the equations, *x* is the horizontal dimension of the opening in mm, *a* is the shear span of the beam in mm, *h* is the vertical dimension of the opening in mm, *d* is the effective depth of the beam in mm, f_{cu} is compressive strength in MPa, A_o is the area of the opening in mm^2 and A_s is the shear area in mm^2. The ultimate shear force of the beam (y_1) was the only output variable in equation 16 that was related to the input variables during prediction using equation 17. The output is experimental results based on Augustino et al. [6].

$$y_1 = F_u \tag{16}$$

$$f(x_1, x_2, x_3) = f(y_1) \tag{17}$$

To ensure that the trained data are not memorised during the learning process [17], data were divided randomly into 3:1:1, that is, 60% for training, 20% for validation, and 20% for testing. The selection of hidden nodes and hidden layers is crucial as it affects the accuracy of the ANN model. In practice, these hidden nodes and layers are always done in trial and error; nevertheless, due to less input database, the study by Isleem [53] and Schmidhuber [54] proposed that a single hidden layer with enough neurons, as in Figure 18, is enough. Therefore, the additional hidden layer does not offer practical benefits. For this case, the number of hidden neurons should range between the number of input and output neurons. The study by Hinton et al. [55] and Heaton [56] suggested the best way of anticipating the number of hidden neurons in a single hidden layer that predicts the output parameters well. Using Equation 18, three (3) hidden neurons were used to predict the shear resistance of the deep concrete beam.

$$h = \frac{2}{3} h_{input} + h_{output} \tag{18}$$

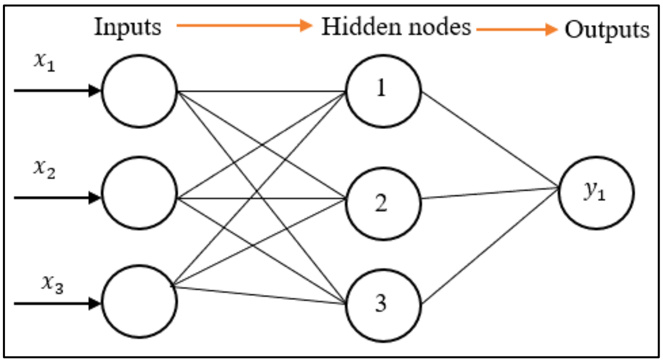

Figure 18. Architecture of the ANN model

The training function Levenberg–Marquardt denoted by Trainlm [57] was selected as the training function. The transfer functions in the hidden and output layers were Tansig and Purelin, respectively. The performance indicator was a mean squared error (MSE). The ANN model performed reasonably and acceptably by transforming data in the input and output ANN layers using the function (Equations 19 and 20) and choosing Purelin transfer functions.

$$x = [x_1, x_2, x_3]^T \tag{19}$$

$$y = [y_1]^T \tag{20}$$

After the ANN model was built, the input and output (shear forces) layers were normalised (Table 7) using Equations 21 to 23 [58, 59], and the network was ready for training. In the ratio of 3:1:1, i.e., training, validation and testing data, the test and validation data are usually not involved in the training process. The validation dataset was used to tell the properness of the training data in each epoch chronologically. In contrast, test datasets provide an unbiased final model performance metric in terms of accuracy and precision after the training process. The optimal number of iterations (epochs) in performing the training was found to be four (4) with a good performance indicator, i.e., minimum mean squared error (refer to Figure 19).

$$X_{norm} = \frac{x_i - x_{min}}{x_{max} - x_{min}} \tag{21}$$

$$Y_{norm} = \frac{y_i - y_{min}}{y_{max} - y_{min}} \tag{22}$$

$$y = Y_{norm}(y_{max} - y_{min}) + y_{min} \tag{23}$$

where, x_i and y_i are input and output to be nnormalised respectively, x_{min} and y_{min} are minimum input and output variables, respectively, x_{max} and y_{max} are maximum input and output variables, respectively and y is the predicted shear resistance based on the normalized-trained dataset as in Table 8. Note that the input (x_1, x_2 and x_3) and y_1 desired output (target) for a given set of inputs are as explained in above. The predicted shear capacity, y_2, is the trained desired output.

Table 7. Scaling of the data

Input/output	φ	f_{cu}, MPa	A_o/A_s	F_u, N
Maximum	0.6488	75	0.2487	170005
Minimum	0.4989	65	0.1220	44316
Mean	0.6026	70.71	0.1537	105371.8
Standard deviation	0.0615	4.99	0.0553	33700.88

Table 8. Inputs, Targets and predicted data in the ANN model

	Beam type	x, mm	h, mm	Fu, N	Ao mm^2	As mm^2	x/a	h/d	x_1	x_2	x_3	y_1	Predicted, y_2N
Experimental Results													
Without fibres	BC1	160	86	78000	13760	112800	0.533	0.229	0.619	65	0.122	78000	83520
	BC2	115	120	84000	13800	112800	0.383	0.319	0.649	65	0.122	84000	87516
	BC3	86	160	76000	13760	112800	0.287	0.426	0.644	65	0.122	76000	86907
	BC4	165	170	74000	28050	112800	0.550	0.452	0.499	65	0.249	74000	49142
With fibres	BS1	160	86	143000	13760	112800	0.533	0.229	0.619	75	0.122	143000	134765
	BS2	115	120	154800	13800	112800	0.383	0.319	0.649	75	0.122	154800	138761
	BS3	86	160	131000	13760	112800	0.287	0.426	0.644	75	0.122	131000	138152
	BS4	165	170	102000	28050	112800	0.550	0.452	0.499	75	0.249	102000	100387
With fibre mesh	*BS1	160	86	127000	13760	112800	0.533	0.229	0.619	75	0.122	127000	134765
	*BS2	115	120	131900	13800	112800	0.383	0.319	0.649	75	0.122	131900	138761
	*BS3	86	160	124500	13760	112800	0.287	0.426	0.644	75	0.122	124500	138152
	*BS4	165	170	90000	28050	112800	0.550	0.452	0.499	75	0.249	90000	100387
Finite Element Model Results													
Without fibres	BC1	160	86	80300	13760	112800	0.533	0.229	0.619	65	0.122	80300	83520
	BC2	115	120	86600	13800	112800	0.383	0.319	0.649	65	0.122	86600	87516
	BC3	86	160	80600	13760	112800	0.287	0.426	0.644	65	0.122	80600	86907
	BC4	165	170	77300	28050	112800	0.550	0.452	0.499	65	0.249	77300	49142
With fibres	BS1	160	86	146500	13760	112800	0.533	0.229	0.619	75	0.122	146500	134765
	BS2	115	120	160600	13800	112800	0.383	0.319	0.649	75	0.122	160600	138761
	BS3	86	160	140400	13760	112800	0.287	0.426	0.644	75	0.122	140400	138152
	BS4	165	170	95200	28050	112800	0.550	0.452	0.499	75	0.249	95200	100387
With fibre mesh	*BS1	160	86	155200	13760	112800	0.533	0.229	0.619	75	0.122	155200	134765
	*BS2	115	120	161900	13800	112800	0.383	0.319	0.649	75	0.122	161900	138761
	*BS3	86	160	146500	13760	112800	0.287	0.426	0.644	75	0.122	146500	138152
	*BS4	165	170	107800	28050	112800	0.550	0.452	0.499	75	0.249	107800	100387

Augustino et al. [6]													
Without fibres	BC1	160	86	79160	13760	112800	0.533	0.229	0.619	65	0.122	79160	83520
	BC2	115	120	82940	13800	112800	0.383	0.319	0.649	65	0.122	82940	87516
	BC3	86	160	82350	13760	112800	0.287	0.426	0.644	65	0.122	82350	86907
	BC4	165	170	54600	28050	112800	0.550	0.452	0.499	65	0.249	54600	49142
With fibres	BS1	160	86	124200	13760	112800	0.533	0.229	0.619	75	0.122	124200	134765
	BS2	115	120	130100	13800	112800	0.383	0.319	0.649	75	0.122	130100	138761
	BS3	86	160	129200	13760	112800	0.287	0.426	0.644	75	0.122	129200	138152
	BS4	165	170	85600	28050	112800	0.550	0.452	0.499	75	0.249	85600	100387
With fibre mesh	*BS1	160	86	125500	13760	112800	0.533	0.229	0.619	75	0.122	125500	134765
	*BS2	115	120	131490	13800	112800	0.383	0.319	0.649	75	0.122	131490	138761
	*BS3	86	160	130560	13760	112800	0.287	0.426	0.644	75	0.122	130560	138152
	*BS4	165	170	86000	28050	112800	0.550	0.452	0.499	75	0.249	86000	100387
Kong and Shark [2]													
Without fibres	BC1	160	86	70183	13760	112800	0.533	0.229	0.619	65	0.122	70183	83520
	BC2	115	120	69284	13800	112800	0.383	0.319	0.649	65	0.122	69284	87516
	BC3	86	160	64223	13760	112800	0.287	0.426	0.644	65	0.122	64223	86907
	BC4	165	170	47446	28050	112800	0.550	0.452	0.499	65	0.249	47446	49142
Ibrahim et al. [7]													
Without fibres	BC1	160	86	90557	13760	112800	0.533	0.229	0.619	65	0.122	90557	83520
	BC2	115	120	90399	13800	112800	0.383	0.319	0.649	65	0.122	90399	87516
	BC3	86	160	90557	13760	112800	0.287	0.426	0.644	65	0.122	90557	86907
	BC4	165	170	51000	28050	112800	0.550	0.452	0.499	65	0.249	51000	49142
Hussein & Abbas [4]													
Without fibres	BC1	160	86	84877	13760	112800	0.533	0.229	0.619	65	0.122	84877	83520
	BC2	115	120	94045	13800	112800	0.383	0.319	0.649	65	0.122	94045	87516
	BC3	86	160	101148	13760	112800	0.287	0.426	0.644	65	0.122	101148	86907
	BC4	165	170	72670	28050	112800	0.550	0.452	0.499	65	0.249	72670	49142
Kong et al. [8]													
With fibres	*BS1	160	86	100315	13760	112800	0.533	0.229	0.619	75	0.122	100315	134765
	*BS2	115	120	103370	13800	112800	0.383	0.319	0.649	75	0.122	103370	138761
	*BS3	86	160	93471	13760	112800	0.287	0.426	0.644	75	0.122	93471	138152
	*BS4	165	170	44316	28050	112800	0.550	0.452	0.499	75	0.249	44316	100387
Smarzewski [5]													
With fibres	*BS1	160	86	163020	13760	112800	0.533	0.229	0.619	75	0.122	163020	134765
	*BS2	115	120	170005	13800	112800	0.383	0.319	0.649	75	0.122	170005	138761
	*BS3	86	160	166569	13760	112800	0.287	0.426	0.644	75	0.122	166569	138152
	*BS4	165	170	136567	28050	112800	0.550	0.452	0.499	75	0.249	136567	100387

In the table, the shear span, a=300 mm, effective depth of the beam, d=376 mm, x is the length of the opening, h is the height of the opening, Ao is the area of the opening, As is the shear area (axd) and Fu is the ultimate shear force

The results in Figures 19 and 20 show the regression models and validation performance, respectively. The trained data in the ANN model had an R^2 of 0.84, indicating a good prediction as compared to the analytical model by Augustino et al. [6] which had an average R^2 of 0.73. The trained, validated and tested had a mean absolute error (MAE) of 11.4, 7.0, and 12.2% with a minimum mean squared error of 0.01, indicating the model's good performance.

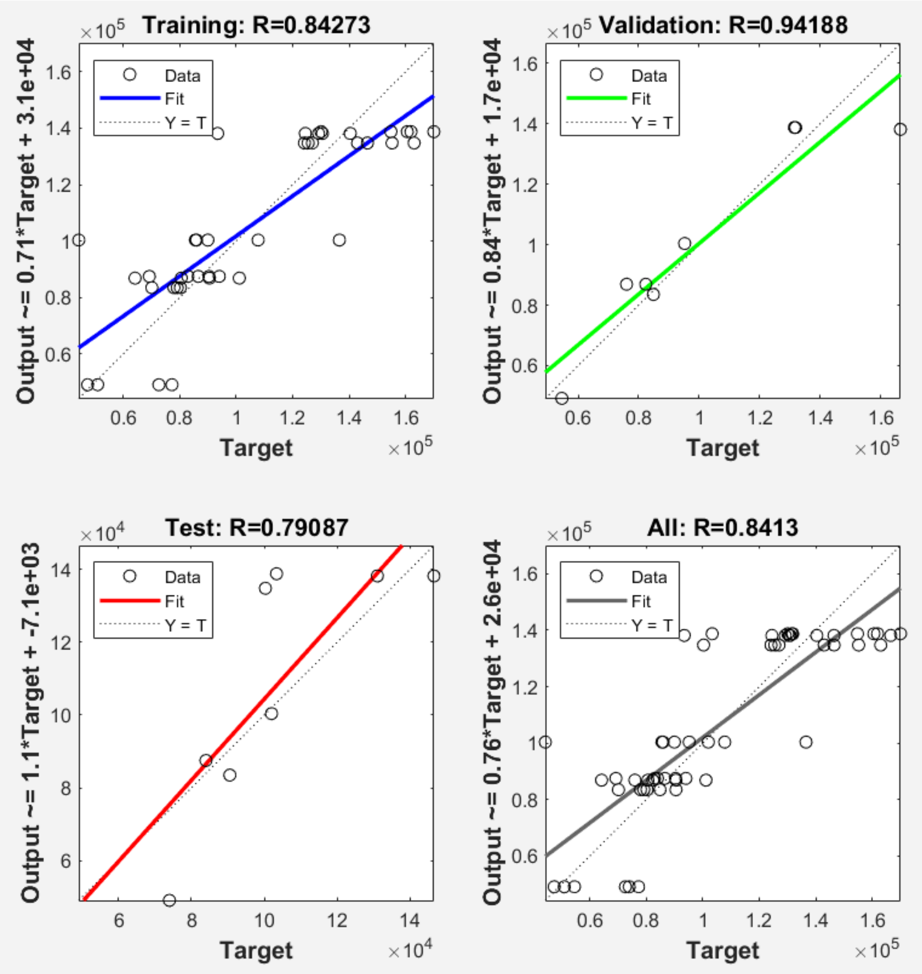

Figure 19. Regression models for training, validation and testing

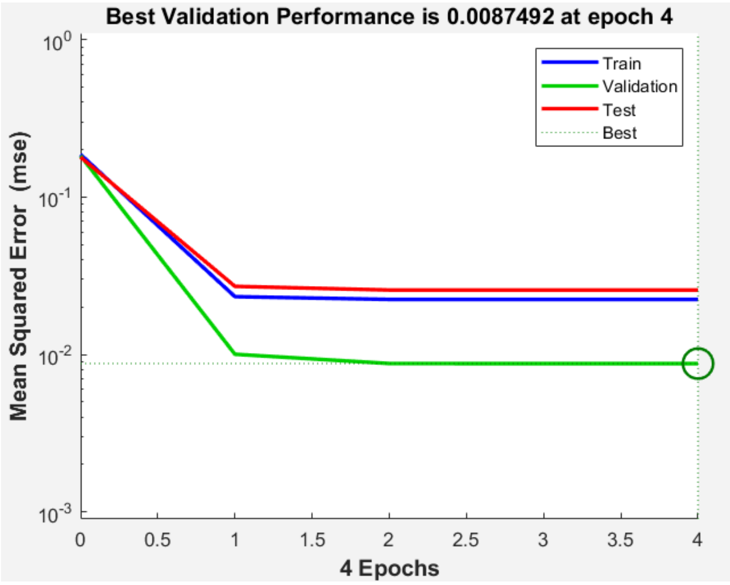

Figure 20. Validation performance

3.7. Sensitivity Analysis on ANN Model

The sensitivity analysis was performed after the training process was completed. This analysis aimed to check the influence of each input on the training network. This involves the determination of network error as in Equation 24 [60]. The process involves deleting one input at a time and training the remaining parameters. In each step, the new network error ($Error_i$) is established. The network error is expected to increase at each step of eliminating the parameter. Thus, to assess the influence of eliminated input, the quotient W in Equation 25 was used to evaluate the sensitivity of each parameter.

$$Error_o = \frac{1}{N}\sum_{i=0}^{N}(y_2 - y_1)^2 \tag{24}$$

$$W = \frac{Error_i}{Error_o} \tag{25}$$

where, $Error_o$ is a network error with all input parameters, N is the number of target outputs, y_2 is the predicted shear capacities through training (trained desired output), y_1 is the desired output(target), W is quotient to assess the sensitivity and $Error_i$ is a new network error at i^{th} deletion of input parameters.

Results in Figure 21 and Table 9 are the sensitivity analysis of the input parameters used in the ANN model. The compressive strength of concrete (x_2) had a high error on its deletion in the network, concluding its importance in determining the shear resistance of the deep concrete beam. The literature confirms this on the significant impact of compressive strength on concrete's mechanical properties [61]. The ratio of opening area to shear area (x_3) seems insignificant in predicting the shear resistance of the deep concrete beam due to an error value of less than 1.0 [60]. Therefore, the order of influence of input parameters in the ANN model is as follows: Compressive strength of concrete > Orientation factor of the traverse opening > Ratio of the opening area to shear area.

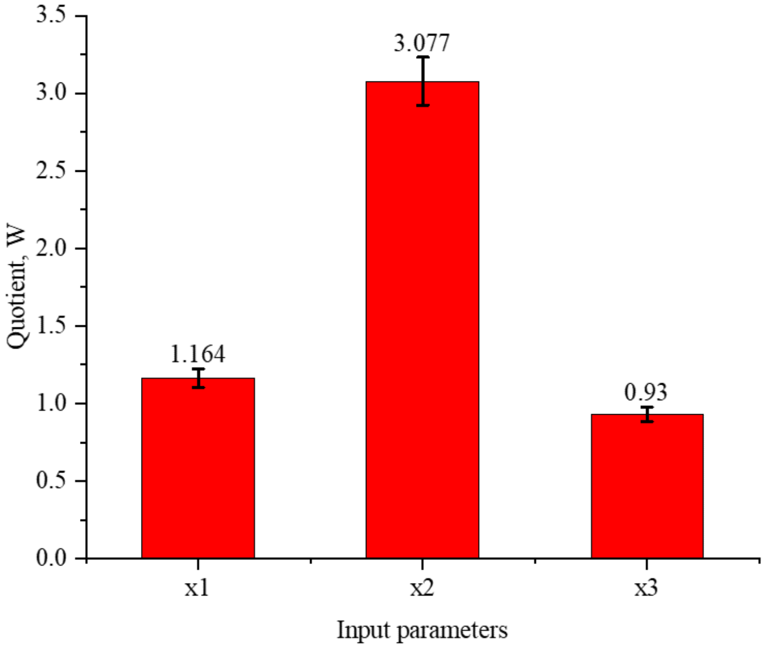

Figure 21. Sensitivity analysis of ANN model

Table 9. Sensitivity analysis of ANN model

	$\sum_{i=0}^{N}(y_2 - y_1)^2$	**Error**	**Quotient, *W***	**Ranking**
All variables	18481350484	330024115.8		
Orientation factor of traverse Opening, x_1	21519002035	384267893.5	1.164363073	2
Compressive strength of concrete, x_2	56870866625	1015551190	3.077202971	1
The ratio of opening to the shear area, x_3	20007988766	357285513.7	0.929782373	3

4. Conclusions and Recommendations

Generally, the following conclusions were established in this study.

- The results of this study show that concrete with fibres has high post-cracking behaviours, such as strain hardening and tension stiffening, that lead to high inelastic crushing and cracking strains, respectively, compared to concrete without fibres.
- In addition, beams without fibres and traverse openings of 86×160 and 165×170 mm failed with the crushing of lower and upper load paths. Only beams with fibres and traverse openings of 165×170 mm follow the same failure trend. It was also noted that beams with fibre meshes had explicit lower and upper load paths regardless of the opening size. Finally, the results show that deep concrete beams with fibres and traverse openings of 160×86, 115×120 and 86×160 mm failed by diagonal-splitting between the loaded points and nearest corners of the opening. All these failure modes in the FE model and experimental work were in close agreement.

- The depth of the neutral axis from the bottom was lower due to high tensile forces below the neutral axis as a total contribution of tensile bars and steel fibres. These forces require less lever arm to balance the counterpart compression forces. This led to a high compression area, resulting in a high shear resistance of the beam.
- The compression steel reinforcement in the boundary strut had high compressive strains for the beam with a square opening. This was due to the stiffness contribution of the remaining depth of concrete above the opening and less interruption of the strut width. The traverse opening depth of more than 0.4D causes nonlinear stress transfer above it, resulting in the rotation of the opening that changes the strain distribution to tensile stains. In addition, this square opening shows less strain in the main bar at the mid-span of the beam compared to other openings.
- The shear resistance based on the finite element model and experimental was close. Therefore, structural engineers in the industry should consider the use of modelling rather than experimental shear tests of the deep concrete beam as they involve resources. In addition, through experiment, it is difficult to explore the strains along steel reinforcements, but using the finite element model, the strains along main steel reinforcements were established that can enable practising engineers to be aware of possible areas that require more attention on detailing to mitigate unforeseen serviceability issues in the beam.
- ANN model predicts reasonably well the shear resistance with R^2 of 0.84 compared to the available analytical model previously reported in Augustino et al. [6]. Based on the selected input parameters in the ANN model, the sensitivity analysis concludes that compressive strength of concrete greatly influences the prediction of the shear resistance of the deep concrete beam, followed by the orientation factor of the traverse opening.

On application, the use of the ANN and FEM models could be of advantage in terms of sustainable construction since the prediction does not involve the environmental degradation of natural resources such as aggregates. Despite this beneficial aspect, the ANN model requires a vast database to increase accuracy. Therefore, the current model can be extended to improve the precision of predicting the opening effect of deep concrete beams that often govern the overall shear performance of these beams for the benefit of practising structural engineers. This study gives an insight into construction materials such as concrete and how their mechanical properties around the opening (D-region) can be improved using waste tyre steel fibres.

5. Declarations

5.1. Data Availability Statement

The data presented in this study are available in the article.

5.2. Funding

The author received no financial support for the research, authorship, and/or publication of this article.

5.3. Conflicts of Interest

The author declares no conflict of interest.

6. References

[1] Augustino, D. S., Kabubo, C., Kanali, C., & Onchiri, R. O. (2022). The orientation effect of opening and internal strengthening on shear performance of deep concrete beam using recycled tyre steel fibres. Results in Engineering, 15, 100561. doi:10.1016/j.rineng.2022.100561.

[2] Kong, F. K., Robins, P. J., & Sharp, G. R. (1975). Design of Reinforced Concrete Deep Beams in Current Practice. Structural Engineer, 53(4), 173–180.

[3] Dang, T. D., Tran, D. T., Nguyen-Minh, L., & Nassif, A. Y. (2021). Shear resistant capacity of steel fibres reinforced concrete deep beams: An experimental investigation and a new prediction model. Structures, 33, 2284–2300. doi:10.1016/j.istruc.2021.05.091.

[4] Hussein, L. T., & Abbas, R. M. (2022). A Semi-Empirical Equation based on the Strut-and-Tie Model for the Shear Strength Prediction of Deep Beams with Multiple Large Web Openings. Engineering, Technology and Applied Science Research, 12(2), 8289–8295. doi:10.48084/etasr.4743.

[5] Smarzewski, P. (2018). Analysis of failure mechanics in hybrid fibre-reinforced high-performance concrete deep beams with and without openings. Materials, 12(1). doi:10.3390/ma12010101.

[6] Augustino, D. S., Kanali, C., Onchiri, R. O., & Kabubo, C. (2023). Simplified shear equation of deep concrete beam considering orientation effect of opening and mechanical properties of fibre-concrete interface. Heliyon, 9(3), 14441. doi:10.1016/j.heliyon.2023.e14441.

[7] Ibrahim, M. A., El Thakeb, A., Mostfa, A. A., & Kottb, H. A. (2018). Proposed formula for design of deep beams with shear openings. HBRC Journal, 14(3), 450–465. doi:10.1016/j.hbrcj.2018.06.001.

[8] Kong, F. K., & Sharp, G. R. (1977). Structural idealization for deep beams with web openings. Magazine of Concrete Research, 29(99), 81–91. doi:10.1680/macr.1977.29.99.81.

[9] Saleh, M., AlHamaydeh, M., & Zakaria, M. (2023). Finite element analysis of reinforced concrete deep beams with square web openings using damage plasticity model. Engineering Structures, 278, 115496. doi:10.1016/j.engstruct.2022.115496.

[10] ABAQUS. (2014). Analysis User's Guide Volume V: Prescribed Conditions, Constraints & Interactions. ABAQUS. Providence, United States.

[11] Saabye, N., & Petersson, H. (1992). Introduction to the finite element method. Pearson, London, United Kingdom.

[12] Schneidera, T., Hua, Y., Gaob, X., Dumasc, J., Zorina, D., & Panozzoa, D. (2019). A Large-Scale Comparison of Tetrahedral and Hexahedral Elements for Finite Element Analysis. arXiv preprint arXiv:1903.09332.

[13] ABAQUS. (2014). ABAQUS/CAE 6.14 User's Manual. Abaqus. Providence, United States.

[14] MATLAB. (2012). MATLAB and Statistics Toolbox Release 2012b; The MathWorks, Inc., Natick, Massachusetts, United States.

[15] Sandeep, M. S., Tiprak, K., Kaewunruen, S., Pheinsusom, P., & Pansuk, W. (2023). Shear strength prediction of reinforced concrete beams using machine learning. Structures, 47, 1196–1211. doi:10.1016/j.istruc.2022.11.140.

[16] Amani, J., & Moeini, R. (2012). Prediction of shear strength of reinforced concrete beams using adaptive neuro-fuzzy inference system and artificial neural network. Scientia Iranica, 19(2), 242–248. doi:10.1016/j.scient.2012.02.009.

[17] Awolusi, T. F., Oke, O. L., Akinkurolere, O. O., Sojobi, A. O., & Aluko, O. G. (2019). Performance comparison of neural network training algorithms in the modeling properties of steel fiber reinforced concrete. Heliyon, 5(1), 1115. doi:10.1016/j.heliyon.2018.e01115.

[18] Huang, X., Cao, H., & Jia, B. (2023). Optimization of Levenberg Marquardt Algorithm Applied to Nonlinear Systems. Processes, 11(6), 1794. doi:10.3390/pr11061794.

[19] Sakamoto, H., Matsumoto, K., Kuwahara, A., & Hayami, Y. (2005). Acceleration and stabilization techniques for the Levenberg-Marquardt method. IEICE Transactions on Fundamentals of Electronics, Communications and Computer Sciences, E88-A(7), 1971–1977. doi:10.1093/ietfec/e88-a.7.1971.

[20] Farber, R. (2011). CUDA Application Design and Development. Elsevier, Amsterdam, Netherlands.

[21] Saleh, M., AlHamaydeh, M., & Zakaria, M. (2023). Shear capacity prediction for reinforced concrete deep beams with web openings using artificial intelligence methods. Engineering Structures, 280, 115675. doi:10.1016/j.engstruct.2023.115675.

[22] Isleem, H. F., Chukka, N. D. K. R., Bahrami, A., Oyebisi, S., Kumar, R., & Qiong, T. (2023). Nonlinear finite element and analytical modelling of reinforced concrete filled steel tube columns under axial compression loading. Results in Engineering, 19. doi:10.1016/j.rineng.2023.101341.

[23] Yap, S. P., Bu, C. H., Alengaram, U. J., Mo, K. H., & Jumaat, M. Z. (2014). Flexural toughness characteristics of steel-polypropylene hybrid fibre-reinforced oil palm shell concrete. Materials and Design, 57, 652–659. doi:10.1016/j.matdes.2014.01.004.

[24] Augustino, D. S., Onchiri, R. O., Kabubo, C., & Kanali, C. (2022). Mechanical and Durability Performance of High-Strength Concrete with Waste Tyre Steel Fibres. Advances in Civil Engineering, 2022. doi:10.1155/2022/4691972.

[25] Mohamed, M. A. S., Ghorbel, E., & Wardeh, G. (2010). Valorization of micro-cellulose fibers in self-compacting concrete. Construction and Building Materials, 24(12), 2473–2480. doi:10.1016/j.conbuildmat.2010.06.009.

[26] Shelote, K. M., Gavali, H. R., Bras, A., & Ralegaonkar, R. V. (2021). Utilization of co-fired blended ash and chopped basalt fiber in the development of sustainable mortar. Sustainability (Switzerland), 13(3), 1–19. doi:10.3390/su13031247.

[27] Li, L., Xia, J., Chin, C., & Jones, S. (2020). Fibre distribution characterization of ultra-high performance fibre-reinforced concrete (Uhpfrc) plates using magnetic probes. Materials, 13(22), 1–20. doi:10.3390/ma13225064.

[28] Le, A. T., & Le Hoang, A. (2023). Comparisons of flexural, split tensile, double punch, and direct tension tests on high-performance concrete reinforced with different fiber types. Case Studies in Construction Materials, 19, 2413. doi:10.1016/j.cscm.2023.e02413.

[29] ACI 318-19. (2019). Building Code Requirements for Structural Concrete (ACI 318-19): An ACI Standard; Commentary on Building Code Requirements for Structural Concrete (ACI 318R-19). American Concrete Institute (ACI), Michigan, United States.

[30] Wang, H., Zhang, C., & Wu, H. (2023). Shear Capacity Prediction Model of Deep Beam Based on New Hybrid Intelligent Algorithm. Buildings, 13(6). doi:10.3390/buildings13061395.

[31] Le Nguyen, K., Thi Trinh, H., Nguyen, T. T., & Nguyen, H. D. (2023). Comparative study on the performance of different machine learning techniques to predict the shear strength of RC deep beams: Model selection and industry implications. Expert Systems with Applications, 230, 120649. doi:10.1016/j.eswa.2023.120649.

[32] Abaqus. (2014). Abaqus 6.11 Theory Manual. Dassault Systèmes Simulia Corp., Providence, United States.

[33] Kanos, A., Kanos, A., Perdikaris, P. (2006). Size Effect on Concrete Splitting Tensile Strength and Modulus of Elasticity. Measuring, Monitoring and Modeling Concrete Properties, Springer, Dordrecht, Netherlands. doi:10.1007/978-1-4020-5104-3_29.

[34] Rai, P. (2021). Non-Linear Finite Element Analysis of RC Deep Beam Using CDP Model. Advances in Technology Innovation, 6(1), 01–10. doi:10.46604/aiti.2021.5407.

[35] Rutner, M. P. (2010). Using composite behavior to improve the blast resistance of columns in buildings. Blast Protection of Civil Infrastructures and Vehicles Using Composites, 342–374, Woodhead Publishing, Sawston, United Kingdom. doi:10.1533/9781845698034.2.342.

[36] Van der Aa, P. J. (2014). Biaxial Stresses in Steel Fibre Reinforced Concrete Modelling the Pull-Out Behaviour of a Single Steel Fibre using FEM. Master Thesis, Eindhoven University of Technology, Eindhoven, Netherlands.

[37] Joosten, M. W., Dingle, M., Mouritz, A., Khatibi, A. A., Agius, S., & Wang, C. H. (2016). A hybrid embedded cohesive element method for predicting matrix cracking in composites. Composite Structures, 136, 554–565. doi:10.1016/j.compstruct.2015.10.030.

[38] EN 1992-1-1. (2004). Eurocode 2: Design of concrete structures - Part 1-1: General rules and rules for buildings. European Committee for Standardization, Brussels, Belgium.

[39] Shahnewaz, M., & Alam, M. S. (2014). Improved shear equations for steel fiber-reinforced concrete deep and slender beams. ACI Structural Journal, 111(4), 851–860. doi:10.14359/51686736.

[40] Slater, E., Moni, M., & Alam, M. S. (2012). Predicting the shear strength of steel fiber reinforced concrete beams. Construction and Building Materials, 26(1), 423–436. doi:10.1016/j.conbuildmat.2011.06.042.

[41] Hsu, L. S., & Hsu, C. T. T. (1994). Complete stress – strain behaviour of high-strength concrete under compression. Magazine of Concrete Research, 46(169), 301–312. doi:10.1680/macr.1994.46.169.301.

[42] Wahalathantri, B. L., Thambiratnam, D. P., Chan, T. H. T., & Fawzia, S. (2011). A material model for flexural crack simulation in reinforced concrete elements using ABAQUS. First International Conference on Engineering, Design and Developing the Built Environment for Sustainable Wellbeing, Queensland University of Technology, Brisbane, Australia.

[43] Qin, X., Huang, X., Li, Y., & Kaewunruen, S. (2024). Sustainable design framework for enhancing shear capacity in beams using recycled steel fiber-reinforced high-strength concrete. Construction and Building Materials, 411, 134509. doi:10.1016/j.conbuildmat.2023.134509.

[44] Lantsoght, E. O. L. (2019). How do steel fibers improve the shear capacity of reinforced concrete beams without stirrups? Composites Part B: Engineering, 175(July), 107079. doi:10.1016/j.compositesb.2019.107079.

[45] Mansur, M. A., & Alwis, W. A. M. (1984). Reinforced fibre concrete deep beams with web openings. International Journal of Cement Composites and Lightweight Concrete, 6(4), 263–271. doi:10.1016/0262-5075(84)90021-6.

[46] Alsaeq, H. M. (2013). Effects of opening shape and location on the structural strength of RC deep beams with openings. International Journal of Civil and Environmental Engineering, 7(6), 494–499.

[47] Mohamed, A. R., Shoukry, M. S., & Saeed, J. M. (2014). Prediction of the behavior of reinforced concrete deep beams with web openings using the finite element method. Alexandria Engineering Journal, 53(2), 329–339. doi:10.1016/j.aej.2014.03.001.

[48] Al-Ahmed, A. H. A., & Khalaf, M. R. (2017). Openings effect on the performance of reinforced concrete deep beams. Proceeding of the First MoHESR and HCED Iraqi Scholars Conference in Australasia, 5-6 December, 2017, Melbourne, Australia.

[49] Schlaich, J., Schaefer, K., & Jennewein, M. (1987). Toward a Consistent Design of Structural Concrete. PCI Journal, 32(3), 74–150. doi:10.15554/pcij.05011987.74.150.

[50] Li, L. (2019). Fibre Distribution Characterization and its Impact on Mechanical Properties of Ultra-high Performance Fibre Reinforced Concrete. PhD thesis, The University of Liverpool, Liverpool, United Kingdom.

[51] Peng, F., Cai, Y., Yi, W., & Xue, W. (2023). Shear behavior of two-span continuous concrete deep beams reinforced with GFRP bars. Engineering Structures, 290, 116367. doi:10.1016/j.engstruct.2023.116367.

[52] Abadel, A., Alenzi, S., Almusallam, T., Abbas, H., & Al-Salloum, Y. (2023). Shear behavior of self-consolidating concrete deep beams reinforced with hybrid of steel and GFRP bars. Ain Shams Engineering Journal, 14(9), 102136. doi:10.1016/j.asej.2023.102136.

[53] Isleem, H. F., Augustino, D. S., Mohammed, A. S., Najemalden, A. M., Jagadesh, P., Qaidi, S., & Sabri, M. M. S. (2023). Finite element, analytical, artificial neural network models for carbon fibre reinforced polymer confined concrete filled steel columns with elliptical cross sections. Frontiers in Materials, 9. doi:10.3389/fmats.2022.1115394.

[54] Schmidhuber, J. (2015). Deep Learning in neural networks: An overview. Neural Networks, 61, 85–117. doi:10.1016/j.neunet.2014.09.003.

[55] Hinton, G. E., Osindero, S., & Teh, Y.-W. (2006). A Fast Learning Algorithm for Deep Belief Nets. Neural Computation, 18(7), 1527–1554. doi:10.1162/neco.2006.18.7.1527.

[56] Heaton, J. (2015). Deep learning and neural networks. Heaton Research, Incorporated, Chesterfield, United States.

[57] Demuth, H. B., & Beale, M. H. (2000). Neural network toolbox: for use with MATLAB: user's guide. The MathWorks, Inc., Natick, Massachusetts, United States.

[58] Sheela, K. G., & Deepa, S. N. (2013). Review on Methods to Fix Number of Hidden Neurons in Neural Networks. Mathematical Problems in Engineering, 2013, 1–11. doi:10.1155/2013/425740.

[59] Rachmatullah, M. I. C., Santoso, J., & Surendro, K. (2021). Determining the number of hidden layer and hidden neuron of neural network for wind speed prediction. PeerJ Computer Science, 7, e724. doi:10.7717/peerj-cs.724.

[60] Mrzygłód, B., Hawryluk, M., Janik, M., & Olejarczyk-Wożeńska, I. (2020). Sensitivity analysis of the artificial neural networks in a system for durability prediction of forging tools to forgings made of C45 steel. The International Journal of Advanced Manufacturing Technology, 109(5–6), 1385–1395. doi:10.1007/s00170-020-05641-y.

[61] Hasan, B. A., & Saeed, J. A. (2023). Effect of Concrete Strength on Shear Capacity of Reinforced High-Strength Concrete Continuous Beams without Web Reinforcements. Advances in Civil Engineering, 8784575. doi:10.1155/2023/8784575.